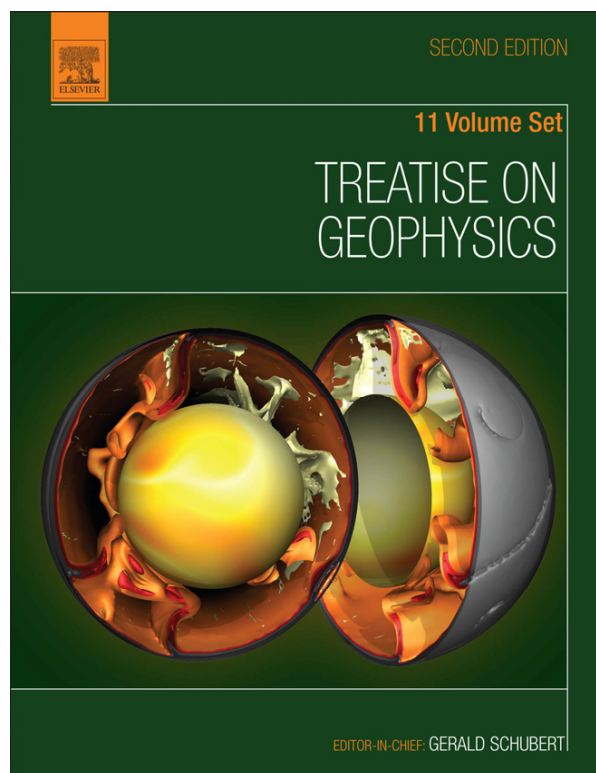


Provided for non-commercial research and educational use.
Not for reproduction, distribution or commercial use.

This article was originally published in *Treatise on Geophysics, Second Edition*, published by Elsevier, and the attached copy is provided by Elsevier for the author's benefit and for the benefit of the author's institution, for non-commercial research and educational use including without limitation use in instruction at your institution, sending it to specific colleagues who you know, and providing a copy to your institution's administrator.



All other uses, reproduction and distribution, including without limitation commercial reprints, selling or licensing copies or access, or posting on open internet sites, your personal or institution's website or repository, are prohibited. For exceptions, permission may be sought for such use through Elsevier's permissions site at:

<http://www.elsevier.com/locate/permissionusematerial>

Tanimoto T., Heki K. and Artru-Lambin J Interaction of Solid Earth, Atmosphere, and Ionosphere. In: Gerald Schubert (editor-in-chief) *Treatise on Geophysics*, 2nd edition, Vol 4. Oxford: Elsevier; 2015. p. 421-443.

4.16 Interaction of Solid Earth, Atmosphere, and Ionosphere

T Tanimoto, University of California, Santa Barbara, CA, USA

K Heki, Hokkaido University, Sapporo, Japan

J Artru-Lambin, Centre National d'Etudes Spatiales, Toulouse, France

© 2015 Elsevier B.V. All rights reserved.

This chapter is a revision of the previous edition chapter by T Tanimoto, J Artru-Lambin, Volume 4, pp. 421–444, © 2007, Elsevier B.V.

4.16.1	Introduction	422
4.16.2	Seismic Noise	423
4.16.2.1	Low-Frequency Peak: Atmospheric Effects	423
4.16.2.1.1	Cause	423
4.16.2.1.2	Turbulence	424
4.16.2.1.3	Reduction of seismic noise	424
4.16.2.2	Hum	425
4.16.2.2.1	Discovery	425
4.16.2.2.2	Seasonal variations	425
4.16.2.2.3	Excitation mechanism	425
4.16.2.2.4	Ubiquitous Rayleigh waves	426
4.16.2.3	Microseisms	426
4.16.2.3.1	Nature of waves	426
4.16.2.3.2	Excitation mechanisms	427
4.16.2.3.3	Source location	428
4.16.2.3.4	Microbaroms	428
4.16.2.3.5	Implication to past climate	429
4.16.2.4	From Noise to Structure	429
4.16.2.4.1	The correlation technique in diffuse wavefield	429
4.16.2.4.2	Related techniques	429
4.16.3	Localized Sources of Interactions	429
4.16.3.1	Historical Context	429
4.16.3.2	Theoretical Preliminaries	430
4.16.3.2.1	Wave propagation in the atmosphere	430
4.16.3.2.2	Frequency–wavelength domains of interest	431
4.16.3.3	Observation Techniques	431
4.16.3.3.1	Surface observation: Seismometer, microbarograph, and hydrophones	431
4.16.3.3.2	High-altitude observation: Ionosondes, Doppler sounding, transmission (GPS), and <i>in situ</i> measurements	432
4.16.3.4	Sources in the Solid Earth	433
4.16.3.4.1	Away from the source: Surface waves and tsunamis	434
4.16.3.4.2	Direct atmospheric waves	435
4.16.3.5	The Case of the Great Sumatra–Andaman Earthquake	436
4.16.3.6	The Cases of the 2011 Megathrust Earthquakes in Tohoku-Oki, Japan	437
4.16.3.7	Sources in the Atmosphere	438
4.16.3.7.1	Eruptions	438
4.16.3.7.2	Sonic boom	439
4.16.4	Conclusion	439
References		439

Nomenclature

C_s	Sound speed	m_e	Electron density
e	Electron charge	N_e	Electron density in the upper atmosphere
f	Frequency in hertz (Hz)	\mathbf{v}	Velocity (three-component vector)
f_1	Primary carrier frequency of GPS	z	Vertical coordinate ($z=0$ is surface and positive upward)
f_2	Secondary carrier frequency of GPS	γ	Specific heat ratio
G	Gravitational constant (6.67×10^{-11} MKS unit)	$\Delta\mathbf{g}$	Perturbation to gravitational acceleration
g	Gravitational acceleration	ΔP	Surface pressure perturbation
k_x, k_y, k_z	Three components of wave number	$\Delta\rho$	Density perturbation
		ζ	Ocean surface displacement

$\bar{\zeta}$	Averaged ocean surface displacement over its wavelength	ω_a	Acoustic cutoff frequency
ρ	Density	ω_g	Brunt-Väisälä frequency
ω	$2\pi f$	ϵ_0	Permittivity of vacuum

4.16.1 Introduction

The atmosphere has been traditionally ignored by seismologists in their analysis of seismograms. Seismologists typically regard the surface of the solid Earth as the upper boundary of the Earth and this boundary is treated as a traction-free boundary. The atmospheric pressure is not zero, however, and the correct boundary condition must reflect the existence of the atmosphere with its diminishing density with height. Strictly speaking, the actual physical upper-boundary condition should be in the atmosphere as the radiation boundary conditions.

Despite this approximate treatment of the surface boundary, seismology has been successful mainly because of two factors. The first is that the impedance contrast at the atmosphere/solid Earth boundary is quite large. Density contrast across this layer is larger than 2000 (1.2 vs. 2700 kg m⁻³) and P-wave velocity contrast is about 20 (300 vs. 6000 m s⁻¹). If we take the case of P-waves impinging on the solid surface from below, there is obviously some transmitted P-wave energy, but the majority of the energy is reflected back into the solid media due to this high impedance ratio. Resulting seismograms hardly indicate the effects of the leakage of transmitted energy.

The second important factor is the low mass of the atmosphere. The mass of the solid Earth is 6.0×10^{24} kg, while the mass of the atmosphere is only 5.1×10^{18} kg. Therefore, phenomena in the solid Earth are affected very little even if we include atmospheric effects in the analysis. It is thus justifiable to ignore the atmosphere and use the free-surface boundary conditions at the solid surface.

But does this mean that there are no benefits to include the atmospheric layer in the analysis? In a nutshell, the purpose of this chapter is to point out that there are many benefits to doing so. We can immediately think of two potential advantages; the first is the possibility of obtaining information on solid Earth processes from analyses of atmospheric waves. It has been pointed out that the eruption of Pinatubo volcano in 1991 generated air-coupled waves that provided information on the nature of the eruption process. Second, some earthquakes have been known to generate Rayleigh wave-coupled airwaves, which provide quantitative information on excitation source processes. These examples are analogous to the use of tsunami for the study of earthquake source process, because even though tsunami themselves are mostly confined to the liquid layer (ocean), their waveforms often provide information about the rupturing process on an earthquake fault. Analyses of atmospheric waves have not been as useful as analyses of tsunami so far, but more careful studies of atmospheric waves may lead to useful applications to understanding solid Earth processes.

Another benefit comes from the analysis of seismic noise. Most seismic noise in seismograms is generated by interactions between the solid Earth and the atmosphere or the ocean. In the past 10 years, such noise was shown to be practically useful because we can recover Green's functions between any pair of stations using a cross correlation technique. Its application to Earth structure study is under way: Seismic noise can provide surface wave dispersion curves between two stations and promise to provide results that were not available from earthquake data. The cross correlation technique also provides information on the flow (direction) of propagating seismic energy, thereby providing potential information about the source location of noise, which was not possible to determine before.

This chapter consists of two main parts: In the first part, we will describe the nature of seismic noise and Green's function cross correlation technique. We will review the study of seismic noise and how noise illuminates our understanding of atmosphere-solid Earth interactions. Since the atmosphere and oceans are strongly coupled and often not separable, the oceans are involved in many of these processes.

In the second part, we will discuss the effects of transient sources in the solid Earth such as earthquakes, volcanic eruptions and large atmospheric explosions, and their resulting effects in the atmosphere. These events radiate energy in various types of waves, such as seismic waves in the solid Earth, tsunamis in the oceans, and internal waves in the atmosphere. Dynamic coupling allows the transmission of a part of the wave energy across the Earth surface, hence the generation of atmospheric, ocean, or tsunami waves from sources external to their respective domains. Sources of such coupled waves include (1) atmospheric explosions, natural (meteors and volcanoes) or man-made, (2) earthquakes, and (3) sonic booms from supersonic jets (Concorde and Space Shuttle). Some notable effects observed after the great Sumatra-Andaman earthquake will also be discussed.

The first and second parts take two different views on modeling the source-medium relationship. The first part follows the view that seismic waves generated by atmospheric effects are generated by surface atmospheric pressure variations. The Earth is basically separated into two distinct media in contact. In this view, generation of acoustic/gravity waves in the atmosphere by sources in the solid Earth is mainly by vertical surface displacement. On the other hand, the second follows the so-called full-coupling approach; there is no artificial boundary between the atmosphere and the solid Earth, and the whole Earth is treated as a single medium. Normal modes are the normal modes of the whole system, and propagating waves cross the atmosphere-solid Earth boundary just like other boundaries inside the Earth. The approach in the first part is an approximation in comparison with a more holistic approach in the second part, but it seems to hold well and tend to provide better physical insights.

4.16.2 Seismic Noise

Peterson (1993) summarized seismic noise characteristics from global distribution of 75 stations. One of the most frequently quoted results from this study is the parameterized model called the new low-noise model (NLNM). Figure 1 shows a plot of this model in the form of acceleration power spectral density. This model has often been used as a reference in the discussion of seismic noise studies.

From the perspective of a seismologist, one of the main features in Figure 1 is the existence of a low-noise frequency band from 2 to 20 mHz (millihertz). Existence of this low-noise band explains why analyses of long-period body and surface waves have been successful in the past few decades as these waves exist in this low-noise band (1 mHz–10 Hz). Detection of small amplitude waves has been possible because of this low-noise characteristic, which is not as easily done outside this frequency band.

From the perspective of a scientist interested in the atmosphere–solid Earth interactions, Figure 1 shows three prominent peaks; from the low-frequency end, they are (1) the low-frequency peak below 0.1 mHz, whose peak is outside the range of this plot but the decreasing trend with frequency up to about 2 mHz is clearly recognized, (2) a small peak or a bump at about 7–10 mHz (denoted as hum in this figure), and (3) large amplitude peak(s) at 0.1–0.2 Hz (microseisms). In this section, we will discuss each of the three peaks from the low-frequency end, particularly focusing on the question which components in the Earth system interact to create these peaks.

The model NLNM was derived from vertical component seismograms. The noise in horizontal components is often an order of magnitude larger than the noise in vertical component because horizontal components are affected by tilts that are generated by temperature variations and atmospheric pressure variations. They are often dominant sources of noise in horizontal component seismograms but are confined to shallow

depths and local regions. In this chapter, noise in horizontal components will not be discussed.

4.16.2.1 Low-Frequency Peak: Atmospheric Effects

Seismic noise below 2 mHz increases toward lower frequencies (Figure 1). This is a global feature that has been confirmed repeatedly from long-period seismographs and gravimeters.

4.16.2.1.1 Cause

The main cause of this noise is density changes in the atmosphere. For example, as weather patterns change, density changes occur in the atmosphere. These changes affect the gravitational field and generate small perturbations in gravitational acceleration at the surface of the Earth.

This mechanism was pointed out by Warburton and Goodkind (1977) by analyzing two collocated instruments, a barometer and a superconducting gravimeter. Barometric (surface pressure) data represent an integration of density anomalies along a vertical column above a station:

$$\Delta P = \int_0^{\infty} \Delta \rho g dz \quad [1]$$

where ΔP is the surface pressure perturbation, $\Delta \rho$ is density perturbation in this formula, and the integration is from the surface of the Earth ($z=0$) to infinity. Effects of atmospheric density perturbations above an observing station can be approximated by a formula similar to the Bouguer gravity formula:

$$\Delta g = 2\pi G \int_0^{\infty} \Delta \rho dz \quad [2]$$

where Δg is the perturbation to gravitational acceleration and G is the gravitational constant. Since g does not vary very much near the surface, barometric data and gravity data are related, to a good approximation, by

$$\Delta g = \frac{2\pi G}{g} \Delta P \quad [3]$$

Warburton and Goodkind showed that collocated gravimeter data and barometric data correlate with coefficients close to a value predicted by $2\pi G/g$.

There is, however, an assumption in using the Bouguer gravity formula; in applying this formula, density perturbation in the atmosphere is assumed to be shaped like a disklike pattern, and density variations laterally away from the station location (in latitude and longitude) do not affect the gravitational acceleration very much. More careful evaluation of such effects, using a meteorologic simulation model, showed that deviation from this formula is small (Boy et al., 1998; Hinderer and Crossley, 2000).

Changes in the atmospheric pressure also cause deformation of the elastic Earth as a surface load. Correction due to this effect is usually added to the aforementioned formula in the analyses (Crossley et al., 1995; Merriam, 1992; Niebauer, 1998; Spratt, 1982; Van Dam and Wahr, 1987; Warburton and Goodkind, 1977). This effect is not negligible and in fact was claimed to be larger than the previously mentioned effect in earlier period of seismic noise study (Sorrells, 1971; Sorrells et al., 1971). But it is smaller than the right-hand side of the aforementioned formula.

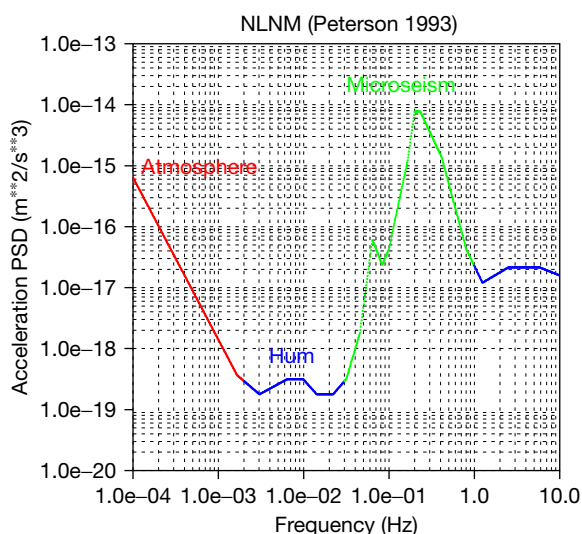


Figure 1 The new low-noise model (NLNM) by Peterson (1993). Power spectral density (PSD) in unit for acceleration is used for this plot. Frequency range is from 1/10000 to 10 Hz.

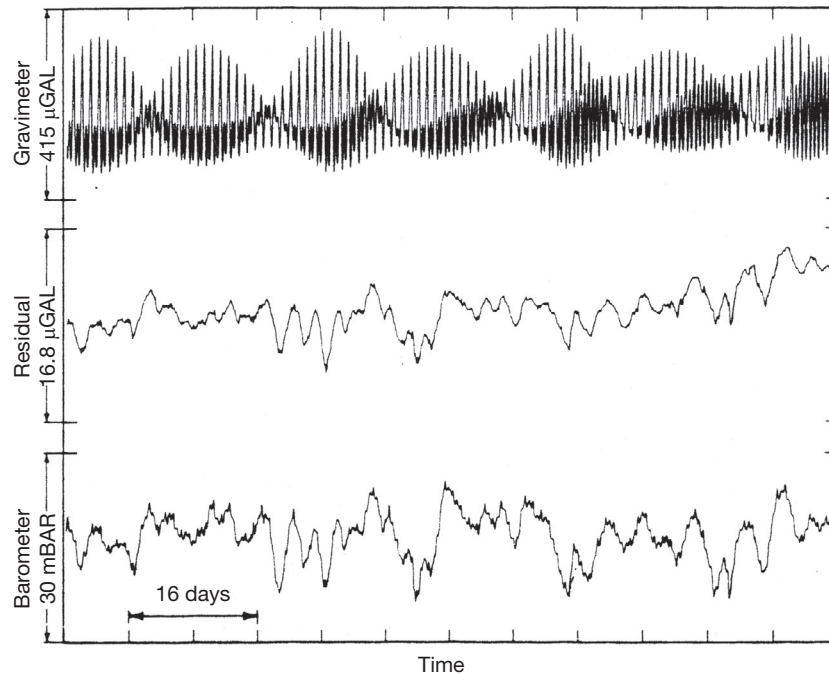


Figure 2 (Top) Original gravity signal from Warburton and Goodkind (1977). Data were recorded by superconducting gravimeter. (Middle) Gravity signal after tidal signal removal. (Bottom) Barometer signal, which correlates well with the trace in the middle.

A clear demonstration of atmospheric pressure effects at the time of a cold front passage was documented by Müller and Zürn (1983), and some careful quantitative computational analysis was reported by Rabbel and Zschau (1985).

Figure 2 shows the evidence of correlation between gravity data and surface pressure data after the removal of tidal signals from gravimeter data. The original gravity record (top) is dominated by tidal signals, but after their removal, the middle trace is obtained. This time series matches the barometric data at the bottom closely, indicating peak-to-peak correlations between the middle trace and the bottom trace.

4.16.2.1.2 Turbulence

While it seems that the correlation between gravity (ground motions) and surface pressure data is good as shown in Figure 2, the correlation coefficient hovers around 0.5 and never becomes close to one. The uncorrelated part of the signal may be due to additional forces, such as wind stress (Reynolds stress) in atmospheric turbulence, which dominates the frequency range above 1 mHz (Tanimoto, 1999). Frequency dependence of surface pressure in this frequency band shows the $1/f$ behavior as observed spectra in Figure 3 show (e.g., Tanimoto and Um, 1999). This $1/f$ behavior is consistent with the prediction by the theory of turbulence with the Kolmogorov-type scaling relation (Landau and Lifshitz, 1987; Tennekes and Lumley, 1971) and directly supports the importance of turbulence in this frequency band.

4.16.2.1.3 Reduction of seismic noise

Existence of the previously mentioned mechanism suggests that, if a seismic/gravity instrument is colocated with a barometer, one can reduce the level of noise considerably by taking advantage of this correlation. For analyses of tidal and

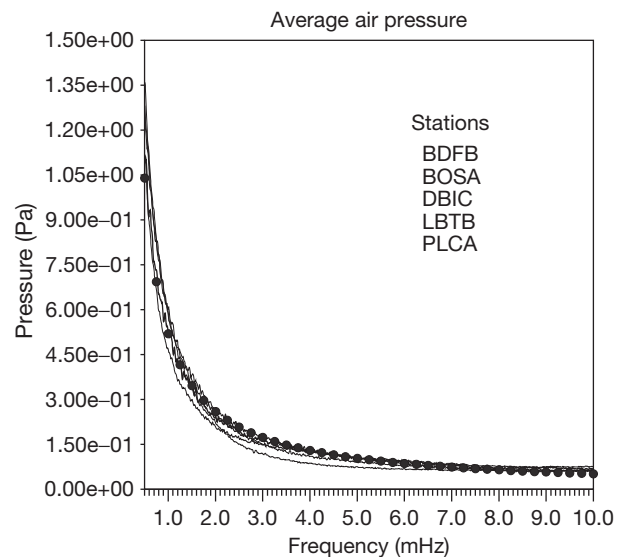


Figure 3 Barometric data (pressure) from five stations in North and South America. Analysis was performed for 20-day-long signals and spectral amplitudes were averaged over 0.2 mHz range. Solid circles denote $1/f$ trend.

lower-frequency data, this has become a common practice since the study of Warburton and Goodkind (1977). For seismic data, especially for normal-mode studies (about 1 mHz and above), Zürn and Widmer (1995), Beauquin et al. (1996), and Roult and Crawford (2000) showed significant noise reduction. These studies showed that noise level below 1 mHz can be made lower than the model NLNM by this correlation technique.

4.16.2.2 Hum

The second peak denoted by hum in [Figure 1](#) was identified as a broad peak by [Peterson \(1993\)](#). It was shown later that this peak is associated with multiple modal peaks, primarily on the left-hand side of its maximum. [Figure 4](#) shows an example from data in this frequency range, obtained from global network data by averaging 11 stations located at various parts of the world. The bottom panel is an enlarged figure within the small box in the top panel and shows that modal peaks exist for the frequency range between 2 and 7 mHz. They are shown to match the eigenfrequencies of fundamental spheroidal modes almost exactly, as the eigenfrequencies for the preliminary reference Earth model (PREM; [Dziewonski and Anderson, 1981](#)) are drawn in the bottom panel by vertical lines. These continuously excited modes are all fundamental spheroidal modes and do not seem to contain any overtone modes. They are now commonly referred to as the Earth's hum.

4.16.2.2.1 Discovery

The discovery of continuously excited modal peaks was made in 1997. A broad peak in Peterson's model has been noted since 1993, or perhaps even earlier, but the hum was discovered as an independent feature from it. The initial reports were by [Suda et al. \(1998\)](#), [Kobayashi and Nishida \(1998\)](#), and

[Tanimoto et al. \(1998\)](#). These and subsequent studies showed that all sites where the noise level is as low as 10^{-18} ($\text{m}^2 \text{s}^{-3}$) in acceleration spectral density (for the frequency band 2–15 mHz) show signals of the hum. Since the global minimum of horizontal noise is an order of magnitude higher than this value, all observations were from vertical component seismograms or gravimeters. The types of seismic instruments that led to these discoveries included broadband seismometers STS-1 and gravimeters with spring sensor (LaCoste–Romberg gravimeters) or superconducting sensors. It was recently shown that seismic data from broadband seismometers STS-2 (with lower pendulum period than STS-1, about 100 s) at the Black Forest Observatory (BFO) in Germany show the hum ([Widmer-Schmidrig, 2003](#)). This may not be surprising, however, since the noise level is as low as 10^{-18} ($\text{m}^2 \text{s}^{-3}$) for STS-2 at this low-noise site. The most important point seems to be that the signal of the hum is observed if the noise level is about 10^{-18} ($\text{m}^2 \text{s}^{-3}$) or less, in unit for acceleration spectral density.

[Nawa et al. \(1998\)](#) reported the existence of the hum in their superconducting gravimeter data at Showa Station in Antarctica. Their report was made before the three papers cited earlier, but the reported results contain peaks from grave spheroidal modes (angular degree < 10) that have not been confirmed independently. In addition, their later study ([Nawa et al., 2000a,b](#)) showed that the noise level at this station seems to be much higher than 10^{-18} ($\text{m}^2 \text{s}^{-3}$) for the frequency band 1–5 mHz.

4.16.2.2.2 Seasonal variations

These modal amplitudes display seasonal variations; claims of the predominant 6-month periodicity were made by [Tanimoto and Um \(1999\)](#) from a frequency-domain analysis and by [Ekström \(2001\)](#) from an entirely independent time-domain analysis. A claim for an annual seasonality was made by [Nishida et al. \(2000\)](#), although they claimed that annual signal was dominant and was thus mildly different from the previously mentioned two studies.

Detection of seasonal variations had major implications for the source of excitation of the hum because it basically removed causes in the solid Earth, because phenomena in the solid Earth do not usually have clear seasonal signatures. Up until these discoveries on seasonality were made, slow earthquakes (e.g., [Beroza and Jordan, 1990](#)) were considered to be one of the major candidates for the cause of the hum.

4.16.2.2.3 Excitation mechanism

The cause of the hum may be in the atmosphere or in the oceans. The atmospheric excitation was advocated by [Kobayashi and Nishida \(1998\)](#), [Tanimoto and Um \(1999\)](#), and [Fukao et al. \(2002\)](#). In these papers, pressure fluctuations in the turbulent atmosphere were postulated as the cause. Modal amplitudes of individual peaks were shown to be explained by the atmospheric excitation model. But there was an uncertain part in this scenario, particularly on the correlation length in atmospheric turbulence within the frequency band (2–7 mHz range). This was critical because the excitation of modes by turbulent atmosphere is proportional to this parameter ([Goldreich and Keeley, 1977](#); [Tanimoto, 1999](#)). The atmospheric excitation mechanism was advocated by assuming that this correlation length was about 1 km or larger

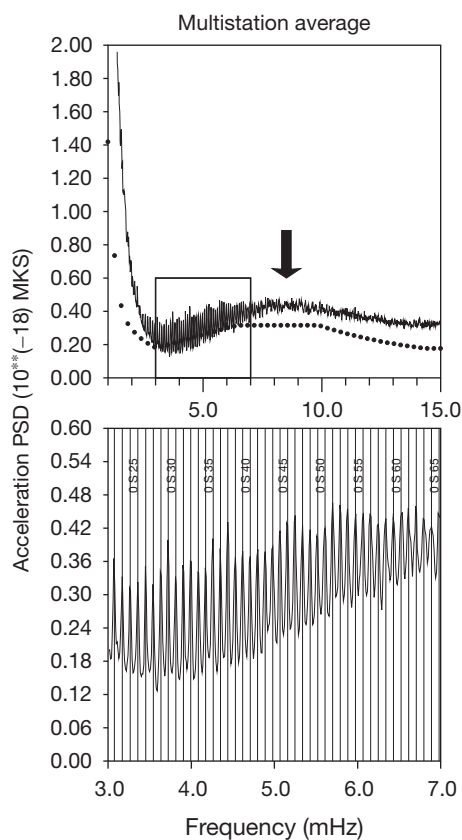


Figure 4 Averaged acceleration PSD from 11 stations, distributed from various parts of the world, is shown at top. Circles in the top panel are NLNM. Spectra in the small box (top) are enlarged in the bottom panel. Each modal peak is shown to match the eigenfrequency of the fundamental spheroidal mode (vertical lines in the bottom panel).

for the frequency band 2–7 mHz. This correlation length has not been confirmed by observation, although the existence of turbulent boundary layer of thickness 1 km seems to imply that it may be a viable candidate.

In addition to this uncertainty in source strength, the atmospheric excitation hypothesis does not provide a good reason for the existence of the broad noise peak between 3 and 15 mHz. In both [Tanimoto and Um \(1999\)](#) and [Fukao et al. \(2002\)](#), this broad spectral peak was assumed to be caused by an unknown background noise, and only the modal peaks above this background noise were modeled by the atmospheric pressure variations at the surface.

The oceanic excitation hypothesis was advanced by [Rhie and Romanowicz \(2004\)](#) and [Tanimoto \(2005\)](#). [Rhie and Romanowicz \(2004\)](#) used seismic array data and located the sources of Rayleigh waves (noise) using two arrays in Japan and California. They found the excitation sources to be in the oceans, especially in the midlatitude bands (30°–60°) in the northern and southern hemispheres. They also claimed that source locations switched rather abruptly between the northern and southern hemispheres. This feature seems to be compatible with general patterns of storm behaviors, although further independent confirmation is desirable.

[Tanimoto \(2005\)](#) showed that the overall spectral shape of the hum, the modal peaks, and the broad spectral peak depicted in [Figure 1](#) (3–15 mHz) can be explained by a single mechanism if the oceanic infragravity waves were the cause. A rather ad hoc feature in the atmospheric excitation hypothesis, which has to find separate causes for modal peaks and for the broad spectral peak, can then be avoided. [Nishida et al. \(2005a,b\)](#) argued that it may still be possible to create this broad peak by atmospheric effects, but a detailed mechanism is still missing in the atmospheric excitation hypothesis.

One of the uncertainties in the oceanic excitation hypothesis lies in our lack of knowledge on the oceanic infragravity waves. A limited number of observations (e.g., [Watada and Masters, 2001](#)) are now supplemented by new observations. Also, some new understanding as to the generation of infragravity waves from oceanic swells is emerging from observation ([Dolenc et al., 2008](#)). Although there have been some studies on the oceanic infragravity waves ([Bromirski and Gerstoft, 2009](#); [Dolenc et al., 2008](#); [Okihiro et al., 1992](#); [Traer et al., 2012](#); [Webb et al., 1991](#)) and many results point to near-coastal generation of waves, a comprehensible, total picture of the generation mechanism seems to be missing. This is still an unresolved question.

Satellite ocean-wave data provide semihemispheric switching of activities, as shown in [Figure 5](#). Ocean waves occasionally reach 10 m or more in high-activity regions, which generates pressure perturbations higher than surface atmospheric pressure. This behavior seems to explain the 6-month periodicity naturally as well as source locations of Rayleigh waves observed by [Rhie and Romanowicz \(2004\)](#). This satellite evidence does not necessarily prove the oceanic excitation mechanism for the hum because strong atmospheric winds are associated with these ocean-wave behaviors and the atmosphere also contains 6-month periodicity. There is clearly an inherent difficulty in the argument of atmospheric versus oceanic excitation because the atmosphere and the oceans are coupled in almost all scales.

It is most likely that the next breakthrough will come from an improved understanding of ocean gravity waves (e.g., [Bromirski and Stephen, 2012](#); [Bromirski et al., 2010](#); [Uchiyama and McWilliams, 2008](#)), although it may take some years.

4.16.2.2.4 Ubiquitous Rayleigh waves

One of the most important notions developed in these studies is that the energy associated with the hum, for the entire frequency range 3–15 mHz, consists of Rayleigh wave energy. From observation, [Nishida et al. \(2002\)](#) showed that signals between 2 and 20 mHz have similar phase velocities to Rayleigh wave phase velocities predicted by the PREM ([Dziewonski and Anderson, 1981](#)). [Nishida et al. \(2009\)](#) performed tomographic inversion from surface wave data retrieved by an application of the cross correlation technique to noise data. The results confirmed consistency with previously derived tomographic results from earthquake data. [Tanimoto \(2005\)](#) showed that the whole spectra in this frequency band can be synthesized by normal-mode summation of spheroidal modes, potentially excited by the oceanic infragravity waves, thereby indicating that they are Rayleigh waves.

While Love waves seem to share some fraction of seismic noise, our understanding of it lags as it is hard to analyze horizontal component data.

4.16.2.3 Microseisms

It has been noted since the early twentieth century that the most obvious and perhaps annoying noise in seismograms is the microseisms with the peak frequency at about 0.1–0.4 Hz ([Figure 1](#)). Amplitudes of this noise were so overwhelming that, before the development of high-dynamic-range digital seismic instruments, seismologists recorded seismic waves separately for high-frequency range (above about 0.5 Hz) and for low-frequency range (below 0.1 Hz) in order to avoid this microseismic noise. World-Wide Standard Seismograph Network, which played the central role for the development of global seismology from the 1960s to 1980s, had such separate (short-period and long-period) instruments.

Modern instruments with high-dynamic-range and digital recordings removed such a cumbersome recording procedure ([Wielandt and Steim, 1986](#)). They record seismic signals from about 1 mHz to 10 Hz using the same sensor. A benefit of such recording procedure is that microseisms are now recorded continuously and this has raised interests among some seismologists since they can now analyze microseism data based on modern high-dynamic-range digital data.

4.16.2.3.1 Nature of waves

A large fraction of secondary microseisms consist of Rayleigh waves with smaller fraction of Love wave energy. This was shown by [Lee \(1935\)](#) and [Haubrich et al. \(1963\)](#) by particle motion analysis, which indicated a characteristic retrograde elliptical particle motion. Later, array analysis ([Capon, 1972](#); [Lacoss et al., 1969](#)) showed that some higher-mode energy and Love wave energy were mixed in the signals. Earlier, [Gutenberg \(1958\)](#) also discussed two types of microseisms, apparently referring to predominant Rayleigh waves and occasional S-waves. From modern three-component data, it is easy to confirm the dominance of Rayleigh waves in microseisms

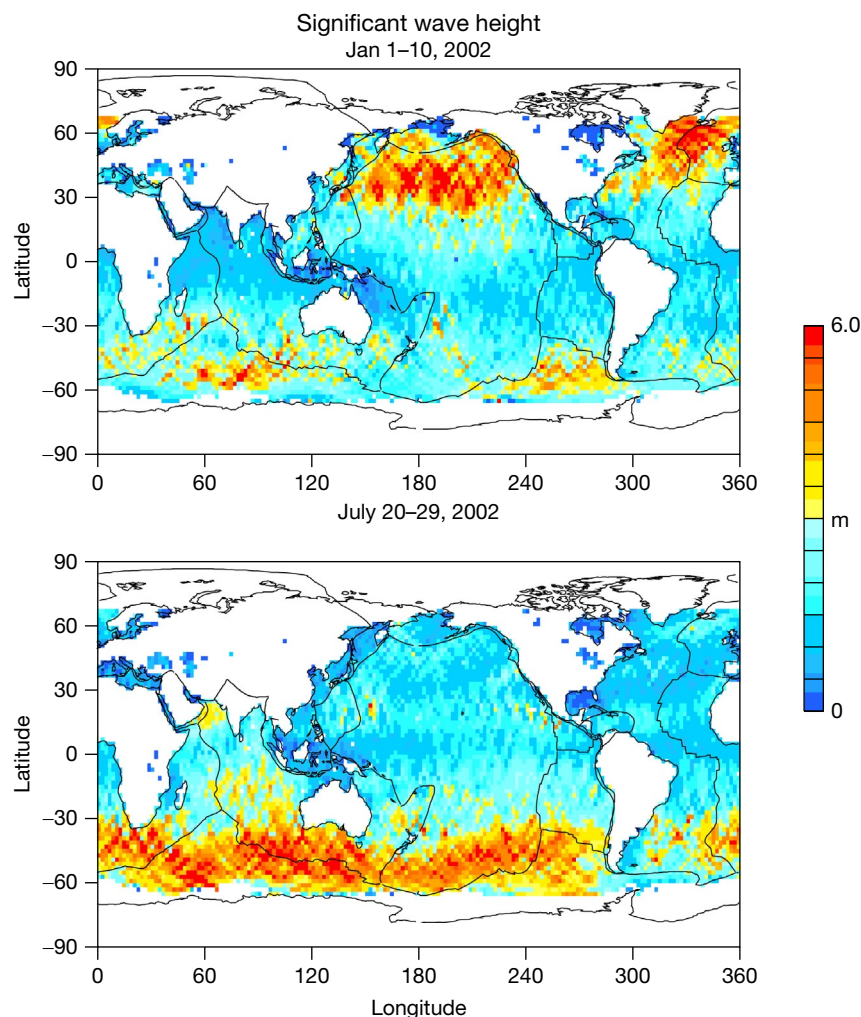


Figure 5 Significant wave height data from TOPEX/Poseidon. Data from two selected periods, one in January (top) and the other in July (bottom), are shown. In January, ocean waves are energetic in the midlatitude region in the northern hemisphere, while ocean waves in the southern hemisphere become energetic in July.

from phase velocity measurements from array observations (Capon, 1972; Lacoss et al., 1969) or from phase-shift observations between horizontal and vertical components, which indicate mostly 90° phase shifts.

Primary microseisms, whose frequency band is about 0.07 Hz, seem to contain a larger fraction of Love waves. This seems to imply different excitation mechanisms between the primary and the secondary microseisms. The commonly accepted mechanism for the secondary microseisms, the wave-wave interaction, is basically a vertical forcing (Longuet-Higgins, 1950), which excited Rayleigh waves much better than Love waves. The mechanism for the primary microseisms is more likely to be interactions of ocean waves with the solid Earth in shallow oceans and thus contains horizontal forcing through topographic coupling (Saito, 2010).

4.16.2.3.2 Excitation mechanisms

One of the important characteristics in microseisms is the fact that larger amplitudes occur for the double-frequency microseisms (0.1–0.4 Hz) than the primary-frequency microseisms

that have the same predominant frequencies with ocean swells (0.05–0.07 Hz). It is still not clear why the double-frequency microseisms have such large amplitudes, but the most widely accepted (basic) mechanism for the double-frequency microseisms is that of Longuet-Higgins (1950). Longuet-Higgins (1950) showed that interactions of two ocean waves in opposite direction can create the double-frequency microseisms through the nonlinear (advection) term in the Navier–Stokes equation. The crux of his theory is that, for surface displacement ζ , pressure perturbation at sea bottom is given by

$$p(t) = \rho \frac{\partial^2}{\partial t^2} \left\{ \frac{1}{2} \zeta^2 \right\} \quad [4]$$

even when the depth extent of colliding waves, which make surface displacement ζ , does not reach the sea bottom. In fact, this pressure arises as a constant in the Bernoulli equation (Longuet-Higgins, 1950), implying that this pressure occurs at all depths. The bar denotes an averaging procedure over a wavelength. For example, if two ocean waves with the same frequency are propagating in opposite directions,

$$\zeta(x, t) = a_1 \cos(\omega t - kx) + a_2 \cos(\omega t + kx) \quad [5]$$

we get

$$p(t) = -\rho a_1 a_2 \omega^2 \cos(2\omega t) \quad [6]$$

from Eqn [4]. This formula contains two important features; first, it shows the occurrence of double-frequency pressure variations. These double-frequency pressure variations at sea bottom generate the double-frequency microseisms. Second, this formula shows that if there exists a unidirectional propagating wave, say, $+x$ meaning $a_2 = 0$, this pressure term goes to zero because it is proportional to $a_1 a_2$. The double-frequency pressure variation requires existence of colliding waves. This mechanism was experimentally confirmed by Cooper and Longuet-Higgins (1951). Phillips (1977) showed a derivation of the same formula from the Navier–Stokes equation by carefully analyzing the vertical momentum balance.

It should be noted, however, that this derivation was made for an incompressible fluid. Compressibility of the ocean is important for the dominant, secondary microseisms (Longuet-Higgins, 1950).

Hasselmann (1963) cast the problem in a more general context, expressing the ocean wave field as a wave number integral and then showing that the predominant term is equivalent to the Longuet-Higgins formula. Normal-mode excitation analysis of seismic wavefields by nonlinear interactions of ocean waves also showed recently that the Longuet-Higgins pressure formula naturally arises from the analysis (Tanimoto, 2007a).

The excitation mechanism for the primary microseisms should be different from the secondary microseisms. Their characteristics are the following: (i) they have the same frequency with ocean waves and (ii) there seems to be a larger fraction of Love waves than secondary microseisms (Friedrich et al., 1998). These characteristics suggest that the excitation is more likely to be through the interactions of ocean waves with the solid Earth at sea bottom, for example, through topographic couplings (Saito, 2010).

4.16.2.3.3 Source location

While it is clear that the nonlinear interactions of ocean waves are necessary to generate microseisms, there is some confusion as to exact locations of excitation sources. There has been a long debate about near-coastal sources versus pelagic sources (in the deep oceans). Near-coastal sources seem common but there seems to be a strong case for some particular pelagic sources (e.g., Cessaro, 1994; Kedar et al., 2008). What we know for sure is the fact that a source must be in a place where ocean-wave collisions occur.

Close relationship between microseisms and ocean swells near the shore was shown by Haubrich et al. (1963), Bromirski et al. (1999), Cessaro (1994), Gerstoft and Tanimoto (2007), Tanimoto (2007b), and Traer et al. (2012). Bromirski et al. (1999) and Tanimoto (2007b) examined a correlation between microseisms from seismograms and ocean waves from buoy data and demonstrated a high correlation and thus a causal relationship. Cessaro (1994) and Gerstoft and Tanimoto (2007) used array analysis from three separate networks and located the sources of microseisms.

It was often conjectured in early studies of microseisms that storms provide a condition that ocean waves collide from opposite directions near their eyes. If this were true, it could be an example of a pelagic source. Tracking of a storm was done by Santo (1960), Sutton and Barstow (1996), and Bromirski (2001) in order to understand the source process of the double-frequency microseisms. The work by Bromirski (2001) provided the best data set and clearly showed that the dominant source area for the double-frequency microseisms was not in the open ocean, where the highest waves occurred, but was near the coast. It seems therefore that standing ocean waves that occur near the coasts, even at the time of large low-pressure system, are the source of double-frequency microseisms. A similar example was shown by Friedrich et al. (1998). This study performed a careful array analysis of seismic data and reported that the primary microseisms contained more Love waves than the double-frequency microseisms, suggesting that the exciting mechanisms may be quite different between them.

Kedar et al. (2008) presented a fairly strong case for a pelagic source in the North Atlantic Ocean. This was based on a comparison between seismic data and hindcase ocean-wave spectral data from the North Atlantic Ocean. They also claimed that there is a preferential ocean depth range, based on the Longuet-Higgins (1950) theory. The source location of this study is close to one of the two areas, pointed out by Cessaro (1994). The other location was in the northeast Pacific, close to Canada and Alaskan coasts. Other recent studies suggested the existence of pelagic sources are Arduin et al. (2011), Hillers et al. (2012), and Zhang et al. (2010).

Schulte-Pelkum et al. (2004) showed a temporary effect of microseismic signals in California caused by ocean waves from the Atlantic Ocean, an evidence for a pelagic source, although occurrence of such phenomena does not seem to be common. Their Atlantic source may have been identical with the source found by Kedar et al. (2008) as this pelagic source seems persistent.

It has also been noted that source area of primary microseisms is often spread out along the coasts, whereas source areas of the double-frequency microseisms appear to be specific locations. This was observed in Europe (Friedrich et al., 1998), on the Atlantic coast (Bromirski, 2001), and on the Pacific coast of the United States (Bromirski et al., 1999; Schulte-Pelkum et al., 2004).

4.16.2.3.4 Microbaroms

Microbaroms are atmospheric low-frequency waves, having frequencies close to those of double-frequency microseisms. The similarity of power spectra to those of microseisms suggests that they are of the same origin (e.g., Donn and Naini, 1973; Nishida et al., 2005a,b). Posmentier (1967) presented a theory analogous to the mechanism proposed by Longuet-Higgins (1950). Arendt and Fritts (2000) published a more complete theory, carefully analyzing various types of waves that arise from interactions of ocean waves. A more elaborate derivation was given by Waxler and Gilbert (2006) who analyzed a two-fluid model (air over seawater) for the radiation of acoustic energy by ocean waves. The basic mechanism in these studies is the same with the Longuet-Higgins mechanism for microseism generation and assumes

interactions of two surface waves propagating in opposite directions. Standing ocean waves near the coasts appear to be generating both microseisms and microbaroms.

4.16.2.3.5 Implication to past climate

Changes in the climate are likely to be related to ocean-wave behaviors (Bromirski and Duennebieer, 2002; Bromirski et al., 1999), which may threaten coastal areas if they become too energetic. However, recovery of past ocean-wave heights from meteorologic data is generally difficult. Grevemeyer et al. (2000) proposed to use activities of microseisms in historical seismograms as a proxy for obtaining information for historical ocean-wave behavior. They reported that the number of high microseismic days increased from 7 to 14 days in the last 50 years and suggested that this may be related to global warming indirectly. While this result should be regarded as preliminary, it is reasonable to expect some correlation, and microseism records may turn out to be a useful source of information for ocean-wave behavior and thus for climate changes.

4.16.2.4 From Noise to Structure

One of the current motivations to study seismic noise is its potential use for Earth structure study. Many techniques have been developed, each focusing on different aspects of data; examples include, in historical order, spatial variation of correlation amplitudes, array analysis for Rayleigh wave phase velocity measurements, use of horizontal-vertical amplitude ratios for Rayleigh wave signals, and the two-station correlation technique to recover Green's functions between a pair of stations. Later, we first discuss the most recent development, the correlation technique to recover Green's functions in diffuse seismic wavefields, and then discuss other techniques under classification as the traditional methods.

4.16.2.4.1 The correlation technique in diffuse wavefield

The first application of the correlation technique to recover structural information was demonstrated in helioseismology (Duvall et al., 1993). The essence of the technique was to recover travel time versus distance curve for multiply reflected waves through cross correlation of data at various distances. In the case of the Sun, seismic sources are stochastic in time and space, and thus, there are no specific noise sources; it can be anywhere and anytime. Therefore, such a technique was most needed and worked effectively to get the results.

Applications to other fields, such as geophysical exploration (Rickett and Claerbout, 1999) and ultrasonics (Weaver and Lobkis, 2001), followed before seismology adopted it recently (Campillo and Paul, 2003). Theoretical basis to recover Green's functions from noise was discussed in Weaver and Lobkis (2001), Lobkis and Weaver (2001), van Tiggelen (2003), Snieder (2004), and Roux et al. (2005a).

Applications to seismic data started with Campillo and Paul (2003). Recovered signals were dominated near the microseismic frequency bands (about period 5–10 s) in earlier demonstrations. The technique was soon applied to local-regional-scale problems such as Southern California (Sabra et al., 2005a,b; Shapiro et al., 2005). It is now applied to

much wider frequency bands (up to 100 s in period) and is also applied to continental-scale structures.

Typical seismic applications first recover Green's functions by cross correlation of seismograms at two stations. Since data are mainly from vertical components and are dominated by Rayleigh waves, traditional dispersion measurements for group velocity are often used to retrieve Earth structure. Dominance of fundamental-mode surface waves in noise is perhaps unavoidable because the excitation sources are in the atmosphere and the oceans, although there are now some studies that report successful recovery of body wave signals (e.g., Roux et al., 2005b). This is currently a rapidly expanding field and the landscape of the research field is expected to change quickly in a few years.

4.16.2.4.2 Related techniques

Aki (1957, 1965) proposed a method, often referred to as the spatial autocorrelation method (SPAC), to determine the local seismic structure. This technique also uses the cross correlation among stations but specifically uses a coherency between two stations; in a flat layered media, the real part of coherency becomes proportional to a Bessel function (Aki, 1965) from which one can obtain phase velocity. Extension of this approach to an attenuating medium was attempted by Prieto et al. (2009), and some theoretical important aspects of the approach were clarified by Tsai (2011).

Lacoss et al. (1969) showed that an array-based phase velocity measurement is a powerful approach. This is basically a beamforming technique, using array data, and is becoming increasingly popular because of availability of dense seismographic networks.

Both SPAC and the beamforming approach are still used at present and an enormous body of literature exists in this area, especially in geotechnical engineering. In geotechnical engineering, the frequency range extends up to 10–20 Hz, exceeding the microseismic frequency band (0.1–0.4 Hz). These studies use not only microseismic signals but also higher-frequency signals generated by other sources and can only be called a cultural noise. A good recent summary of this field was given by Okada (2003).

These traditional techniques have been around 40–50 years, but their practical use may expand as quality and density of seismic instruments have improved recently. We expect to see more use of these methods because there are urgent needs, especially in urban area, to understand near-surface structure as shallow seismic structure plays a critical role for ground motion amplification at the time of major earthquakes.

4.16.3 Localized Sources of Interactions

In this section, we will focus on the interaction between the solid Earth and the atmosphere after localized and transient events such as earthquakes and volcanic eruptions.

4.16.3.1 Historical Context

An early example of observations can be traced back to more than a century ago, the eruption of the Krakatoa volcano (Indonesia) on 26 August 1883. After the eruption, coupled

air–sea waves were observed in barographs and tide gages worldwide (Harkrider and Press, 1967). The meteor or comet explosion in Tunguska (Central Siberia) on 30 June 1908 also induced both atmospheric and seismic waves. The latter was similar in amplitude to a $M=5$ earthquake (Whipple, 1930), although the true source of those waves was an explosion in the air, at an estimated altitude of 8 km (Ben-Menahem, 1975).

The interest for the study of such interactions rose significantly later, during Cold War periods, because atmospheric gravity waves were emitted by nuclear explosions and detection and characterization of such waves became an active research field (Hines, 1972). This led to three major advances during the 1960s. First, a better and efficient theoretical description of internal waves in the atmosphere (Hines, 1960), from the ground up to ionospheric heights, was developed. Second, ionospheric sounding networks capable of monitoring the ionospheric response to those waves (Davies, 1962) were deployed. And third, the occurrence of several major earthquakes (Chile, 22 May 1960, M9.5; Alaska, 28 March 1964, M9.2) revealed the generation of internal acoustic waves in the atmosphere by global Rayleigh wave propagation (Donn and Posmentier, 1964).

More recently, significant advances were made toward a quantitative interpretation and prediction of such coupled phenomena. In particular, new types of atmospheric observations have been made possible by the development of GPS (Global Positioning System) ionosphere monitoring (Calais and Minster, 1998; Mannucci et al., 1998) and by the deployment of the International Monitoring System (global seismological, hydroacoustic, radionuclide, and infrasound network aimed at ensuring compliance with the Comprehensive Nuclear-Test-Ban Treaty). Increased accessibility of numerical computations has also made it possible to refine theoretical modeling of coupled systems (Artru et al., 2004; LePichon et al., 2003).

4.16.3.2 Theoretical Preliminaries

4.16.3.2.1 Wave propagation in the atmosphere

After localized events, energy is transmitted in the form of atmospheric internal waves from the surface to the ionosphere. Those waves arise from the interactions of compressional and gravitational forces and are divided into two classes, long-period gravity waves and short-period acoustic waves. The basic physics of acoustic gravity waves was formulated by Hines (1960), and his formalism is now widely used. Let us review the main features of this theory.

We consider an isothermal atmosphere, initially in hydrostatic equilibrium, and include forces from inertia, gravity, and pressure gradients. We assume that disturbances can be regarded as adiabatic process because wave propagation is a sufficiently fast process. We do not include the effects from the rotation of the Earth, and therefore, large-scale tidal and planetary waves are not considered here. We focus on much shorter-wavelength waves.

Let us use the notations that ρ is the density, p is the pressure, v is the neutral gas velocity, g is the gravitational acceleration, and C_s is the constant sound speed. We then have the following three basic equations: Conservation of mass:

$$\frac{\partial \rho}{\partial t} + v \cdot \nabla \rho = -\rho \cdot \nabla v \quad [7a]$$

Conservation of momentum:

$$\frac{\partial v}{\partial t} + v \cdot \nabla v = g - \frac{1}{\rho} \nabla p \quad [7b]$$

Adiabaticity:

$$\frac{\partial p}{\partial t} + v \cdot \nabla p = C_s^2 \left(\frac{\partial \rho}{\partial t} + v \cdot \nabla \rho \right) \quad [7c]$$

In the equilibrium state, $v_0=0$ and both ρ_0 and p_0 are proportional to $\exp(-z/H)$, where $H=C_s^2/\gamma|g|$ is the density scale height and γ is the specific heat ratio. Assuming ρ_1 , p_1 , and v are small perturbations with no dependency on the y -axis, we may solve the linearized equations as harmonic solutions by assuming that ρ_1 , p_1 , and v are proportional to $\exp[i(\omega t - k_x x - k_z z)]$. The full dispersion relation takes the form

$$\omega^4 - \omega^2 C_s^2 (k_x^2 + k_z^2) + (\gamma - 1) g^2 k_x^2 + i \gamma g \omega^2 k_z = 0 \quad [8]$$

This equation means that, in the presence of gravity, no solution exists in which both k_x and k_z are purely real and different from zero. Let us assume that k_x is real and seek a solution that propagates in the x direction as a harmonic wave. There are now two possibilities, either k_z is purely imaginary or

$$k_z = k'_z + i \frac{\gamma g}{2c^2} = k'_z + i \frac{1}{2H} \quad [9]$$

The first case (k_z pure imaginary) is appropriate for horizontally propagating surface waves, but it permits no variation of phase with height. The second case is appropriate for traveling disturbances in the atmosphere under the influence of gravity. Thus, the second case is pursued here. The dispersion relation can be rewritten as

$$\omega^2 C_s^2 k'_z{}^2 = \omega^4 - \omega^2 \left(C_s^2 k_x^2 + \frac{\gamma^2 g^2}{4C_s^2} \right) + (\gamma - 1) g^2 k_x^2 \quad [10]$$

For a given horizontal wave number, a real solution for k'_z exists only when the right-hand side of Eqn [7], which is a second-order polynomial in ω , is positive. The two roots ω_1 and ω_2 define the following three different cases:

- If $\omega_1 < \omega < \omega_2$, k'_z is purely imaginary. In this case, we can only have waves trapped at the surface propagating only horizontally (Lamb waves).
- If $\omega < \omega_1 < (\gamma - 1)^{1/2} g / C_s$, k'_z is purely real. This corresponds to the internal gravity wave domain, governed primarily by buoyancy. $\omega_g = (\gamma - 1)^{1/2} g / C_s$ is the Brunt–Väisälä frequency.
- If $\omega > \omega_2 > \gamma g / 2C_s$, k'_z is purely real. This corresponds to the internal acoustic wave domain, governed primarily by compression. The high-frequency limit of those waves is usual sound wave (with exponential increase in amplitude). $\omega_a = \gamma g / 2C_s$ is called the acoustic cutoff frequency. In the short-wavelength limit, however, the root ω_2 varies as $C_s k_x$.

Typically, $\omega_a / 2\pi = 3.3$ mHz and $\omega_g / 2\pi = 2.9$ mHz in the lower atmosphere. This classification in acoustic, gravity, and Lamb waves is widely used in aeronomy. It can be extended to nonisothermal models when the scale height is large in comparison with the vertical wavelength. An adaptation of

normal-mode theory to such a nonisothermal model, for the coupled solid Earth–ocean–atmosphere system, has been developed, which allows the simulation of wave propagation for the whole system (Lognonné et al., 1998). The main difference with traditional seismic normal-mode simulation is in the treatment of the upper-boundary condition to reflect the absence of free surface.

Attenuation of waves arises from viscous and thermal dissipations with comparable magnitudes. But except for short-period acoustic waves, attenuation can be neglected up to 100 km of altitude. This is because dominant atmospheric waves that are coupled to Rayleigh waves have frequency content of about 10–20 mHz.

Stronger limitations of this model arise at high altitude because of two reasons; first, amplification with altitude implies that linearized equations will cease to be valid. And second, upward-propagating internal waves eventually reach the ionosphere, where the dynamics is strongly constrained by the influence of magnetic field on charged particles. The ionospheric response to gravity waves is still an object of an extensive literature (Yeh and Liu, 1972).

4.16.3.2.2 Frequency–wavelength domains of interest

Seismic, tsunami, and atmospheric waves result from the action of gravity and elastic forces. Significant effects from both types of forces exist for the relevant frequency range (a few tens of millihertz). Figure 6 represents a normal-mode representation of the whole Earth + ocean + atmosphere system (Artru et al., 2001; Lognonné et al., 1998). The range of existence of seismic, tsunami, acoustic, and gravity waves can be clearly identified, and the different areas where they coexist (seismic and acoustic, tsunami, and gravity) mark the potential

for coupled waves. Outside those area, the dynamic coupling is limited to interface waves (e.g., Lamb wave in the atmosphere).

Study of atmospheric signals caused by sources in the solid Earth is mostly based on observations at the surface (seismograms, barograms, tides gages, and infrasound arrays) or at high altitudes through the ionospheric response to upward-propagating internal waves. The latter measurement can only concern the acoustic or gravity frequency ranges. In particular, seismic and tsunami waves are much more likely to produce strong atmospheric signals at high altitude than many other natural or artificial sources. This is because, despite the very small size of displacements at the surface, they present a unique combination of frequency and horizontal wavelength range necessary for an efficient coupling with internal waves in the atmosphere. On the other hand, major energy from ocean swell, located in the same frequency range, may induce some infrasonic signal trapped at the base of the atmosphere (Garces et al., 2003), but will not in general induce internal (i.e., upward-propagating) acoustic waves in the atmosphere, because the wavelength is much shorter than for Rayleigh waves (Arendt and Fritts, 2000).

4.16.3.3 Observation Techniques

4.16.3.3.1 Surface observation: Seismometer, microbarograph, and hydrophones

Both seismic and pressure sensors have been used to characterize the coupling at the Earth surface. In particular, recent worldwide deployment of infrasound arrays for the International Monitoring System has enabled us to detect atmospheric pressure fluctuations related to solid Earth activity (Figure 7). The frequency band for such instruments is typically between 0.1 and 10 Hz (Mutschlechner and Whitaker, 2005). The noise

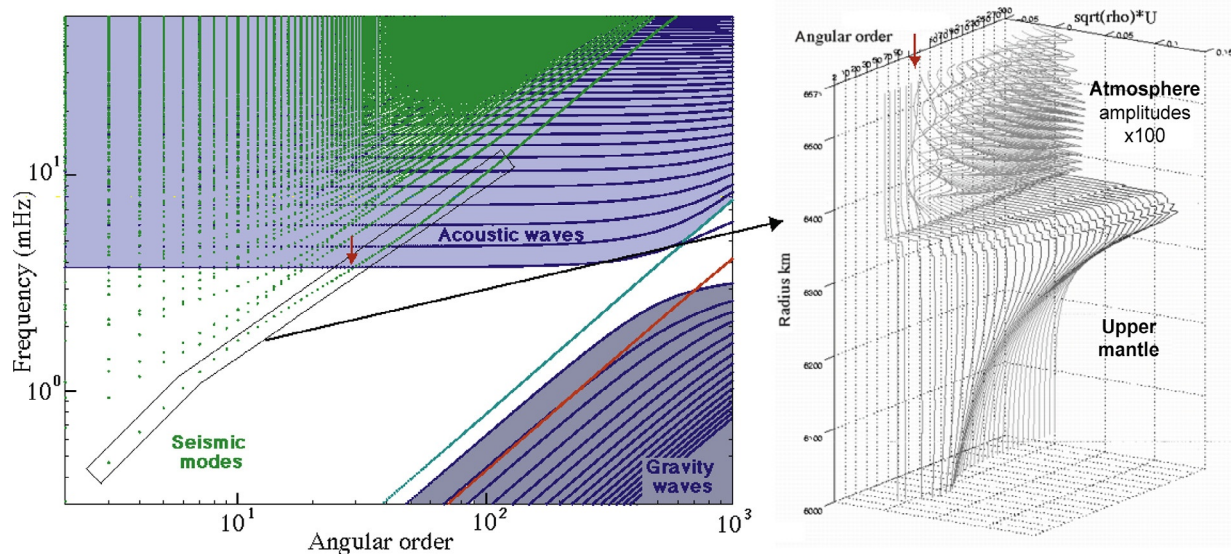


Figure 6 Domains of existence of waves in the solid Earth, ocean, and atmosphere. This figure represents the set of free oscillation modes obtained using standard Minos software (Woodhouse, 1988) for an Earth model composed of the preliminary reference Earth model (PREM) for solid Earth and US Standard Atmosphere 1976 up to 86 km of altitude. Green dots: seismic spheroidal modes; red dots: ‘tsunami’ mode (corresponding to the 3-km ocean layer in PREM); blue dots: acoustic and gravity mode. As Minos software has a free boundary at the top of the model, some obvious errors exist: the atmospheric mode spectrum is not in general discrete because there is no upper-boundary condition, and furthermore, the lowest acoustic branch shown on this plot would correspond to the nonphysical surface atmospheric mode at the top of the model.

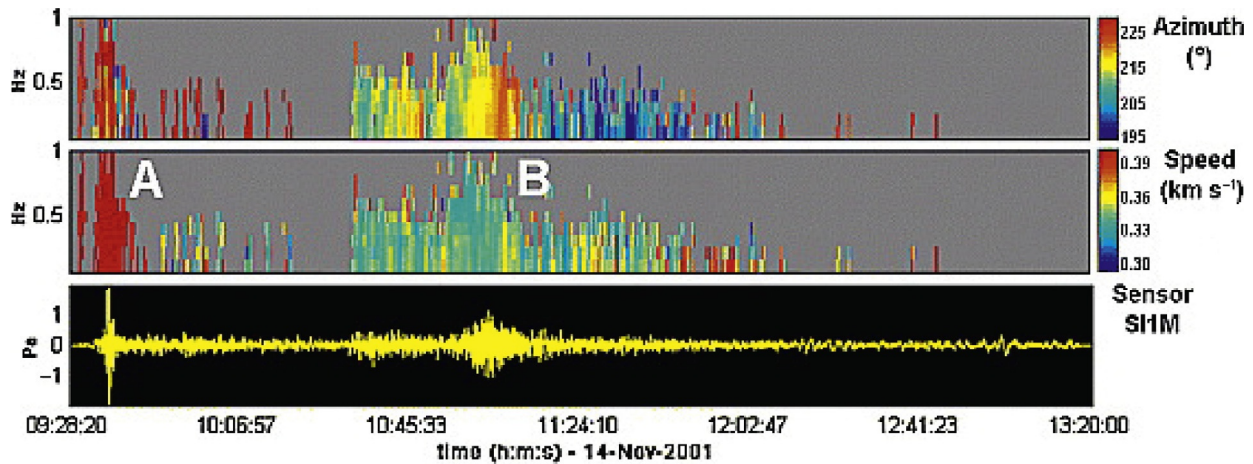


Figure 7 Infrasonic record from the I34MN IMS infrasound array (Mongolia) after the 2011 Kunlun earthquake (Northern China, M_s 8.1 on 14 November 2001). Bottom panel: Atmospheric pressure fluctuations filtered between 0.05 and 4 Hz. Top two panels: The color scales indicate the values of the azimuth and the trace velocity measured at the infrasound station. Y-axis corresponds to frequencies from 0.05 to 1 Hz. In the first part of the signal, coherent wave trains referred to as Group A are related to local seismically coupled air waves. Due to the coupling at the Earth–air interface, the horizontal trace velocity of the ground-coupled airwaves and the seismic waves is identical ($>3 \text{ km s}^{-1}$). Group B corresponds to the propagation of infrasonic waves backscattered by the Kunlun mountain range.

level depends on the wind conditions, from 0.1 to 10 Pa, but it can be reduced by filtering. Those arrays can also be used to determine the azimuth and velocity of the observed signals, which provide information on their origin. Essentially, two types of infrasonic signals are observed after earthquakes (LePichon et al., 2002):

- Seismic coupled air waves, essentially a local conversion of seismic wave vertical motion into sound pressure (Donn and Posmentier, 1964).
- Infrasonic waves remotely generated. Those can be generated at the epicenter (Bolt, 1964) or backscattered by mountain ranges (Young and Greene, 1982).

In the latter case, infrasounds travel obliquely upward in the atmosphere but are reflected or refracted at various altitudes because of sound velocity variations in the atmosphere (Drob et al., 2003). Such a signal arrives later than the coupled air wave and has different azimuth and velocity. Mutschlecner and Whitaker (2005) showed that amplitude of the observed pressure perturbations depend not only on the epicentral distance and magnitude of the earthquake but also on the stratospheric wind speed, which has a major impact on the propagation of infrasounds.

4.16.3.3.2 High-altitude observation: Ionosondes, Doppler sounding, transmission (GPS), and in situ measurements

Detection of acoustic and gravity waves at intermediate altitudes in the neutral atmosphere is not possible due to the absence of *in situ* measurement and because atmospheric remote sensing generally lacks the resolution that would be needed. However, at higher altitudes, in addition to the exponential amplification of the wave amplitude, the interaction with the local plasma leads to perturbations of the ionosphere that are detectable by using radio sounding techniques.

The ionosphere is the intermediate region between the neutral atmosphere and the magnetosphere, ranging

approximately between 60 and 1500 km in altitude. It is a stratified medium, partially ionized by solar radiation (due to ultraviolet light and x-rays). The maximum in electron density is reached between 200 and 400 km of altitude and takes values between 10^5 and $10^7 \text{ e}^{-1} \text{ m}^{-3}$ (Figure 8).

Because it is a plasma, the ionosphere has a strong influence on electromagnetic wave propagation. The plasma frequency is the low-frequency cutoff for radio wave propagation and depends on the local electron density N_e as

$$\omega_p = \left(\frac{N_e e^2}{m_e \epsilon_0} \right)^{\frac{1}{2}} \quad [11]$$

where e and m_e are the electron charge and mass, respectively, and ϵ_0 is the permittivity of vacuum. Typical ionospheric plasma frequencies range from 1 to 20 MHz and their maximum occurs at the maximum of ionization. Ionospheric sounding techniques are based on measurement of either the reflection of radio waves below the maximum plasma frequency or the refraction delay of higher-frequency signals transmitted across the ionosphere from satellites.

4.16.3.3.2.1 Reflection

For frequencies lower than 10 MHz, waves are reflected by the ionospheric layer whose plasma frequency (Eqn [11]) exceeds the frequency of signal. One type of radio sounding of the ionosphere is vertical sounding (ionosonde), measuring the travel time of a reflected signal as a function of frequency. This provides information on the electron density profile. Doppler sounding is based on the measurement of the Doppler shift of monochromatic signal, sent vertically upward and reflected back to the ground. The frequency shift between the emitted wave and the reflected wave is directly proportional to the vertical velocity of the reflecting layer. Using such ionospheric sounding network, Blanc (1985) gave a review of natural and artificial sources of signals recorded in those ‘ionospheric seismometers.’ Both types of sounding can be either ground-based, probing the

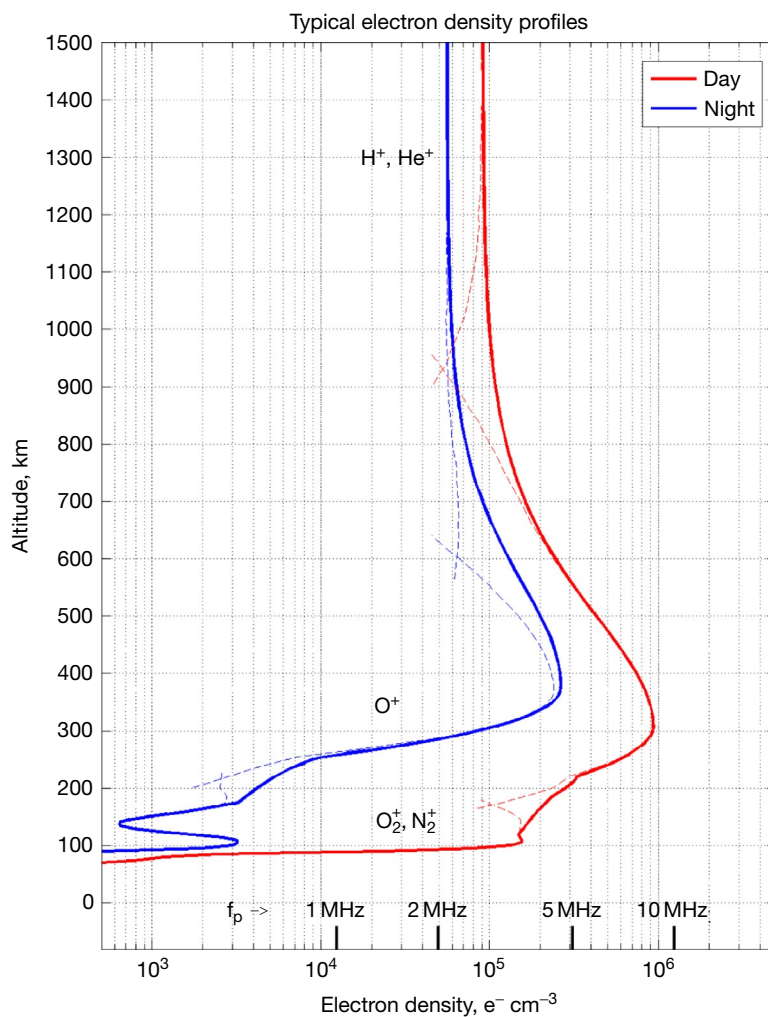


Figure 8 Typical midlatitude electron density profile in the ionosphere. Profiles were obtained using the International Reference Ionosphere model (Bilitza, 2000). Main ions species are indicated (dashed lines are their contribution to ionization), and the plasma frequencies (Eqn [11]) corresponding to different electron densities are indicated.

lower ionosphere up to the electron density maximum, or satellite-based ('top-side sounding').

4.16.3.3.2.2 Transmission

For higher frequencies (typically L-band, 1–2 GHz and higher), electromagnetic waves can propagate across the ionosphere. Ionospheric refraction induces a delay in the travel time, which depends on the frequency of the signal and on the local plasma frequency (Eqn [11]), hence on the local electron density along the ray:

$$\delta_{\rho_{iono}} = \pm \frac{e^2}{4\pi^2 m_e \epsilon_0} \int_{ray} \frac{N_e}{f^2} dl \quad [12]$$

Using travel time measurements at two different frequencies gives access to the total electron content (TEC), which is the integral of electron density along a path between a radio transmitter and a receiver. This measurement on TEC has become widely accessible from the development in satellite altimetry and positioning, since it is a key correction required to be applied to those systems. In particular, GPS relies on

the accurate measurement of satellite–GPS receiver distances and uses a combination of travel time measurements at two frequencies (L1 and L2, respectively, $f_1 = 1.575$ and $f_2 = 1.227$ GHz). Once other sources of error are taken into account (Lanyi and Roth, 1988; Sardon et al., 1994), TEC along the ray can be obtained as a linear combination of the two estimated distances ρ_1 and ρ_2 :

$$TEC = \int_{ray} N_e dl = \frac{1}{40.3} \frac{f_2^2 - f_1^2}{f_2^2 f_1^2} (\rho_1 - \rho_2) \quad [13]$$

4.16.3.4 Sources in the Solid Earth

Ionospheric perturbations that follow earthquakes have been observed both near the seismic source and at teleseismic distances (Figure 9). The first published observations were related to the Great Alaskan Earthquake in 1964. Using ionospheric sounding networks, Bolt (1964) and Davies and Baker (1965) observed atmospheric perturbations propagating from the

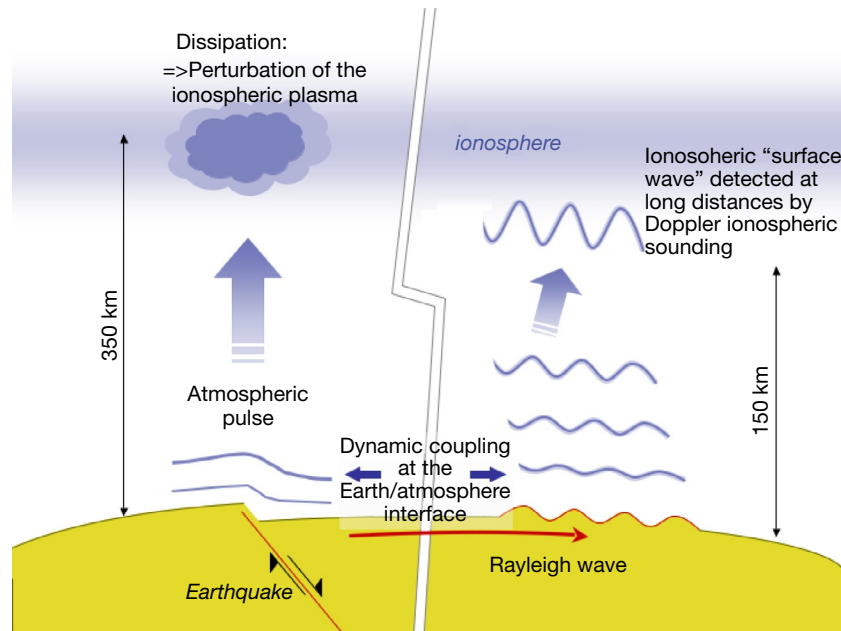


Figure 9 The schematic view of atmospheric waves generated after an earthquake.

epicenter region and the ionospheric signatures of the Rayleigh wave propagation at the sounder location.

4.16.3.4.1 Away from the source: Surface waves and tsunamis

4.16.3.4.1.1 Seismic waves

Seismic surface waves have typical group velocity in the range $3\text{--}4\text{ km s}^{-1}$, whereas the sound velocity in the atmosphere is much smaller (340 m s^{-1}). Therefore, the acoustic wave is sent almost vertically upward and reaches the ionosphere with a delay of 815 min after the passage of Rayleigh waves on the ground. Amplification due to density decrease with altitude can reach $10^4\text{--}10^5$, and attenuation is only observed for short-period signal above 100 km of altitude. Large-scale vertical oscillations of the ionospheric layers can be easily monitored using the Doppler sounding networks described in [Section 4.16.3.3.2](#) ([Blanc, 1985](#); [Yuen et al., 1969](#)). [Figure 10](#) presents a recent example of such measurements. Although monitoring networks are still sparse, such ionospheric oscillations are currently observed systematically for most $M \geq 6.5$ earthquakes worldwide.

Using a normal-mode approach, [Artru et al. \(2001, 2004\)](#) and [Occhipinti et al. \(2010\)](#) had modeled oscillations of ionospheric layers induced by surface Rayleigh waves generated by a major earthquake. Their analysis retrieved source parameters from atmospheric events and showed that atmospheric perturbations generated by surface Rayleigh waves may be amplified by a factor of 10 000 to 100 000 upon attaining heights between 150 and 250 km. Later, [Rolland et al. \(2011a\)](#) investigated the dependence of the coupling efficiency between the solid Earth and the atmosphere on atmospheric conditions. Rayleigh wave-induced ionospheric disturbances were first observed using the dense array of GPS (nowadays, GPS is often rephrased as GNSS (Global Navigation Satellite System) to signify satellite systems for positioning in a general sense) as TEC changes in the

Western United States by [Ducic et al. \(2003\)](#) and [Garcia et al. \(2005\)](#) after the 2002 Denali earthquake in Alaska.

4.16.3.4.1.2 Tsunami waves

Tsunami waves are expected to induce a similar type of coupling with the atmosphere; despite their small amplitude compared with ocean swells, they can generate atmospheric gravity waves because of their long wavelengths. A possibility of detecting tsunami by monitoring the ionospheric signature of the induced gravity waves was proposed by [Peltier and Hines \(1976\)](#). They discussed theoretical issues on the coupling and concluded that it is feasible.

Geometry of tsunami-gravity wave coupling is very different from the coupling between seismic and acoustic waves. Tsunami wave is nondispersive, and its velocity depends only on gravity g and water depth d , as the velocity is given by \sqrt{gd} . From the gravity wave dispersion equation, one can estimate group velocity of the induced gravity wave. Horizontally, it appears to be very close to typical tsunami wave speed, while vertical component is much slower than sound speed (about 50 m s^{-1}). Depending on the period, it would therefore take from one to a few hours for the gravity wave to reach the ionosphere (in contrast to about 10 min for seismic-acoustic waves). The ionospheric perturbation should be behind the tsunami front, with a delay increasing with altitude. Detailed discussion is given in [Occhipinti et al. \(2008, 2011\)](#).

Early papers that proposed using ionospheric measurements to detect tsunami-generating earthquakes ([Najita and Yuen, 1979](#); [Najita et al., 1973](#)) focused on perturbations induced by Rayleigh waves preceding a potentially destructive tsunami. [Artru et al. \(2005\)](#) used ionospheric sounding from a very dense GPS network in Japan (GEONET) to detect the perturbations associated with the arrival of tsunami wave, generated by the 23 June 2001 Peru earthquake. The observed arrival time, wavelengths, and orientation were shown to

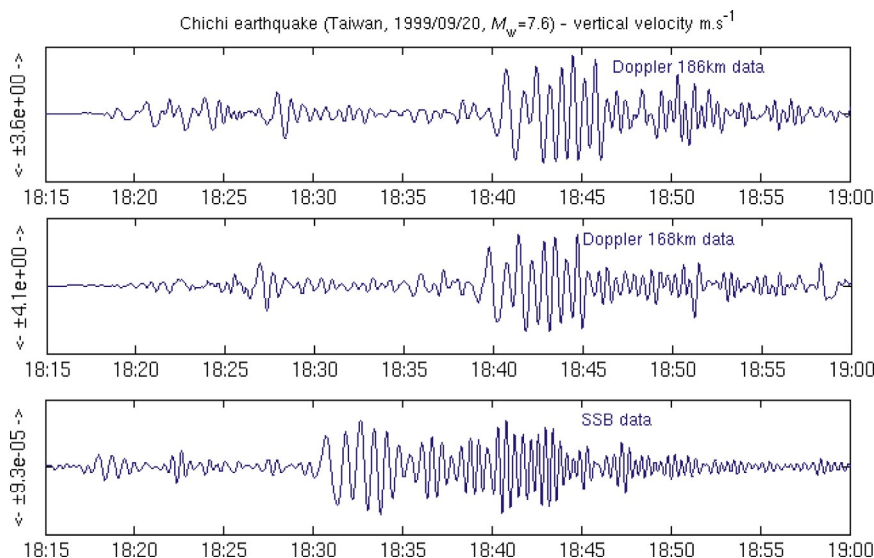


Figure 10 Seismogram and Doppler sounding record (two altitudes: 168 and 186 km) taken in France after Chi-Chi earthquake. Both traces are band-pass filtered between 1 and 50 mHz.

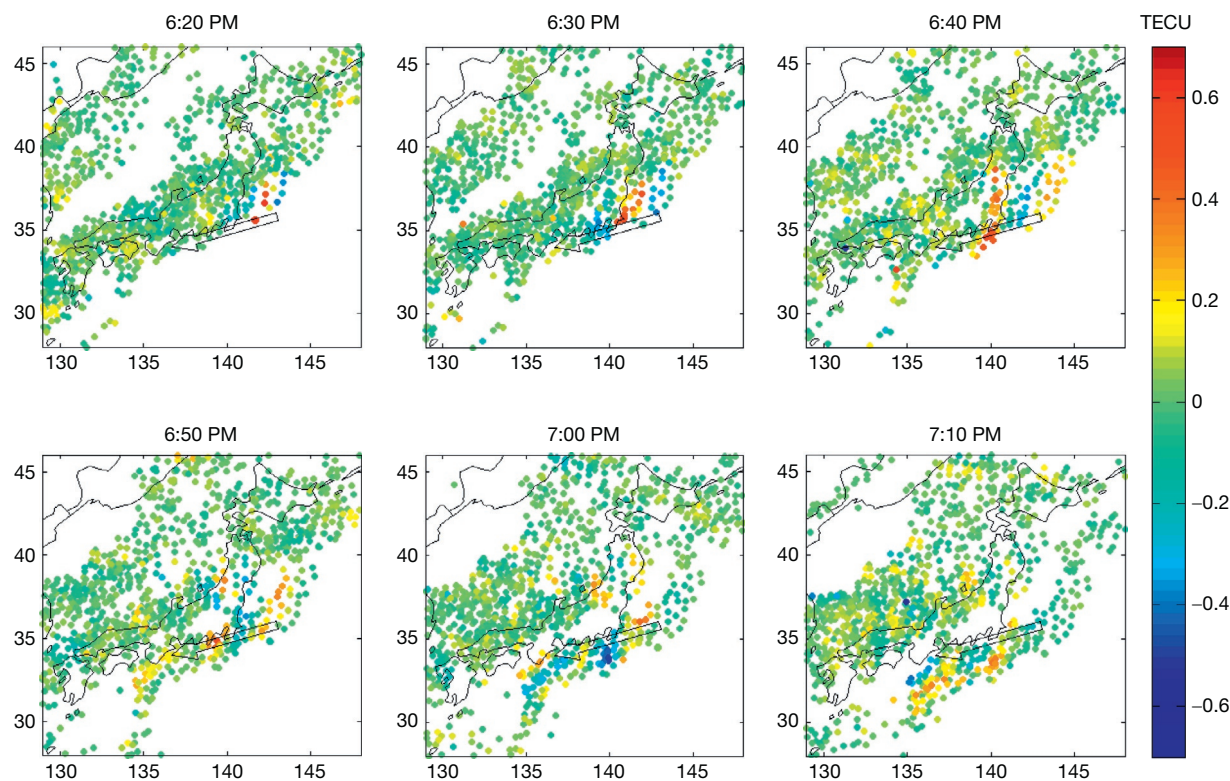


Figure 11 Observed signal for the 23 June 2001 tsunami (initiated offshore Peru): TEC variations plotted at the ionospheric piercing points. A wavelike disturbance is propagating toward the coast of Honshu. This perturbation presents the expected characteristics of tsunami-induced gravity waves and arrives approximately at the same time as the tsunami wave itself.

fit well with theoretical predictions estimated by a simple simulation (Figure 11).

4.16.3.4.2 Direct atmospheric waves

Atmospheric perturbations, observed either at the ground level or in the ionosphere, are often generated away from the

measurement location. Propagation of the signal is therefore essentially in the atmosphere. In most cases, the origin of the atmospheric disturbance is the ground motion near an earthquake source (or an underground nuclear explosion). Calais and Minster (1995) detected perturbations in the ionospheric TEC above Southern California after the Northridge earthquake

($M=6.7$, 17 January 1994) using GPS measurements. [Davies and Archambeau \(1998\)](#) developed a direct modeling of these waves for a simple representation of shallow seismic sources, including high-frequency components of the wave-packet and nonlinear effects. Their results confirmed the seismic origin of the signal, observed after the Northridge earthquake.

The displacement field generated at the Earth's surface produces a piston-like impulse on the atmosphere. [Afrainvich et al. \(2001\)](#) proposed a model for the atmospheric perturbation in the form of 'shock-acoustic waves.' [Drob et al. \(2003\)](#), [Il-Young et al. \(2002\)](#), and [Virieux et al. \(2004\)](#) focused on solving the acoustic wave propagation in order to model data from the CTBT (Comprehensive Nuclear Test Ban Treaty) verification network.

Ionospheric disturbances due to direct acoustic waves were observed by a dense GPS array in Japan after the 2003 Tokachi-Oki earthquake (M_w 8.0) ([Heki and Ping, 2005](#)). Their apparent propagation velocity was much slower (up to 1 km s^{-1}) and could be easily distinguished from the disturbances of Rayleigh wave origin. The interaction with geomagnetic field produced directivity of their propagation. [Heki and Ping \(2005\)](#) suggested it was southward (northward component was suppressed by geomagnetic field) in the midlatitude region of the northern hemisphere. For this earthquake, [Rolland et al. \(2010\)](#) later identified Rayleigh waves in addition to the direct acoustic waves. [Watada et al. \(2006\)](#) analyzed the microbarograph records collocated with seismometers for periods 10–50 s and observed pressure disturbances caused by the acoustic coupling between the atmosphere and the ground beneath the sensors.

Using the Japanese GPS array, after the 1994 Hokkaido-Toho-Oki earthquake (M_w 8.3), [Astafyeva et al. \(2009\)](#) clearly identified two components with distinct velocity contrast, that is, the faster Rayleigh wave component and the slower acoustic wave component. This 1994 earthquake occurred within the subducting slab. Also, two large earthquakes occurred in the central Kuril arc that had different focal mechanisms, that is, a shallow-angle thrust earthquake in 2006 and an outer rise normal-fault earthquake in 2007. [Astafyeva and Heki \(2009\)](#) studied the coseismic ionospheric disturbances of these three earthquakes and found that their waveforms (e.g., polarity of the initial changes) depended on their focal mechanisms.

4.16.3.4.2.1 Other sources of infrasounds

In addition to the coupled surface waves and the direct acoustic shock waves, some atmospheric perturbations related to earthquakes can be observed as scattered waves away from the source. For example, a mountain range can become a source of diffracted infrasound waves at the time of passage of Rayleigh waves ([LePichon et al., 2002, 2003](#); [Mutschlecner and Whitaker, 2005](#)).

Other 'solid Earth' sources of atmospheric infrasounds include avalanches and rockfall ([Bedard, 2000](#)), volcanic activity ([Graces, 1997](#)), and chemical explosions and mining blasts ([Hagerty et al., 2002](#)).

4.16.3.5 The Case of the Great Sumatra–Andaman Earthquake

The great ($M_w=9.1$) Sumatra–Andaman earthquake and tsunami of 26 December 2004 ([Lay et al., 2005](#)) provided a unique opportunity to study solid Earth–ocean–atmosphere

coupling. Indeed, by itself, this particularly large thrust event would generate not only seismic waves and their associated atmospheric Rayleigh waves but also direct atmospheric perturbations. In addition, it triggered an exceptionally large tsunami that propagated across the Indian Ocean. Satellite altimetry observation detected the open-ocean wave, with peak-to-peak amplitude of 40–50 cm ([Song et al., 2005](#)). Tide gauge stations also provided tsunami data, allowing [Tanioka et al. \(2006\)](#) to estimate the rupture process somewhat independently from purely seismic data. The propagation of the tsunami wave across the Indian Ocean lasted several hours, which was enough, according to the tsunami–gravity wave coupling theory described earlier, to generate ionospheric signals. Let us review some recent observations published on the subject.

[Le Pichon et al. \(2005\)](#) and [Garces et al. \(2005\)](#) analyzed infrasound array data. They observed distinct packets of signal arriving successively. The first signal was the pressure perturbation generated at the sensor location by the seismic waves, with horizontal trace velocity greater than 3 km s^{-1} . The second signal was an infrasonic wave train with a mean trace velocity of 0.35 m s^{-1} and a dominant period of 10 s, associated with infrasound radiated from the epicenter region. The third signal consisted of large coherent infrasonic wave, similar in velocity to the previous train, with a dominant period of 30 s. Back azimuth reconstruction indicated a source area extending from the northern tip of Sumatra to the northern margin of the Bay of Bengal. This source area suggests that those infrasonic waves were generated by the tsunami wave, either through the interaction of tsunami with the shoreline or as tsunami reached shallow water and generated shorter-wavelength signals (a few tens of kilometers, comparable to 30 s infrasound waves). [Mikumo et al. \(2008\)](#) analyzed the very low-frequency acoustic gravity waves using microbarographs around the Indian Ocean and in Japan and compared with synthetic barograms generated for a realistic thermal structure in the atmosphere up to 220 km.

At higher altitudes, ionospheric perturbations related to the Sumatra earthquake and tsunami have been reported as well. [Liu et al. \(2006a\)](#) used Doppler sounding network in Taiwan, monitoring the vertical motion of a specific ionospheric layer, and detected two distinct disturbances interpreted as the Rayleigh waves, then to the direct acoustic gravity waves emitted by the crustal motion around the earthquake. Other works published were based on continuous GPS data (i.e., the detection of perturbation in the integrated electron content of the ionosphere), although the distribution of permanent receivers in the Indian Ocean region was quite scarce at the time. [Heki et al. \(2006\)](#) studied the signals related to the direct acoustic gravity waves from the source region and used such observations to retrieve information on the rupture process, in particular the rupture propagation speed. Using the same GPS stations in Sumatra and Thailand, [Otsuka et al. \(2006\)](#) studied the variations of the TEC perturbations between different stations and interpreted the variations as the consequence of directivity in the ionospheric response with respect to the neutral atmosphere perturbation. [DasGupta et al. \(2006\)](#) reported smooth variations in TEC detected by GPS stations located on the east coast of India without giving yet any specific interpretation on their origin. [Iyemori et al. \(2005\)](#) reported a rather different type of observation, using ground-based

fluxgate magnetometer. They observed localized, long-period geomagnetic pulsations in Thailand shortly after the origin time of the earthquake and speculated that they were due to the resonant interaction of magnetic field lines with the upward-propagating magnetosonic waves emitted from the earthquake area. Changes in geomagnetism were also observed in space: Balasis and Manda (2007) detected 30 s pulsation in geomagnetic field associated with the 2004 Sumatra–Andaman and the 2005 Nias earthquakes with a magnetometer on board a low Earth orbiter.

Resonant atmospheric oscillation is considered to occur at frequencies 3.7 and 4.4 mHz (Nishida et al., 2000). Choosakul et al. (2009) found that the atmospheric resonance in these frequencies continued for a few hours in GPS-TEC data taken at Phuket, Thailand, after the 2004 Sumatra–Andaman earthquake.

Searching for the ionospheric disturbances related to the tsunami wave propagation, two studies reported some successful observation. Liu et al. (2006b) used GPS data from five permanent receivers in the southern Indian Ocean and detected traveling ionospheric disturbances with the period in the range 10–20 min, with horizontal propagation speed consistent with the theory of tsunami–gravity wave coupling. Occhipinti et al. (2006) took advantage of the simultaneous sea surface height and TEC measurements provided by altimetry satellites Jason-1 and TOPEX/Poseidon, hence giving data in the open ocean, away from possible coastal perturbation. In addition, they were able to perform a direct three-dimensional (3-D) modeling of the tsunami-generated gravity waves taking into account its interaction with the ionospheric plasma. The simulated and observed perturbations agreed remarkably well considering large uncertainties inherent in combined data sets, models, and theories from very different fields of Earth sciences.

Mai and Kiang (2009) showed that the tsunami-driven gravity wave propagated at the same velocity with the tsunami. Hickey et al. (2009) suggested that the tsunami-driven gravity waves may attain vertical displacements of 2–5 km and electron density perturbations up to 100%. Occhipinti et al. (2008) studied the dependence of the ionospheric signatures of tsunami on geomagnetic field. Hickey et al. (2010) simulated the fluctuations in atmospheric airglow by such gravity waves, which were observed later after the 2011 Tohoku–Oki earthquake (see next chapter).

A suite of large earthquakes have followed the 2004 Sumatra–Andaman earthquake. They include the 2005 M_w 8.6 Nias earthquake (Briggs et al., 2006) and the 2007 M_w 8.5 Bengkulu earthquake (Gusman et al., 2010). Ionospheric disturbances by these earthquakes were studied by Cahyadi and Heki (2013) using a GPS network in Sumatra. The 2007 Bengkulu earthquake showed typical ionospheric responses including the acoustic gravity waves propagating northward with atmospheric resonance at about 5 mHz. However, vigorous plasma bubble activities prohibited near-field observation of ionospheric disturbances by the 2005 Nias earthquake (Cahyadi and Heki, 2012). Later, its ionospheric disturbance was observed in far field by the high-frequency Doppler observations and by an over-the-horizon (OTH) radar system in France, called Nostradamus, by Occhipinti et al. (2010). Coisson et al. (2011) studied how tsunami-induced gravity wave signature appears in OTH radar data.

Ionospheric disturbances by the 2006 Kuril, 2009 Samoa, and the 2010 Chile earthquake tsunamis were reported by Rolland et al. (2010) and Galvan et al. (2011) using GPS data taken in Hawaii, the Western United States, and Japan. In April 2012, a large earthquake (M_w 8.6) occurred off the coast of northern Sumatra (Meng et al., 2012). Studying its ionospheric disturbances is important because of its unique focal mechanism, that is, one of the largest strike-slip earthquakes.

4.16.3.6 The Cases of the 2011 Megathrust Earthquakes in Tohoku–Oki, Japan

The 11 March 2011 Tohoku–Oki earthquake (M_w 9.0) was the first M9 class earthquake that occurred where dense geodetic and geophysical sensors were available. A dense network composed of 1200 continuous GPS stations, GEONET (GNSS Earth Observation Network), has been in operation since the 1990s by GSI (Geospatial Information Authority of Japan) and provided spectacular observing results concerning the coupling of the solid Earth, the atmosphere, and the ionosphere. Shortly after the earthquake, rapid reports on various aspects of ionospheric disturbances were published. In the near field, the concentric wave fronts created by internal gravity waves were clearly identified with GEONET stations (Figure 12) (Rolland et al., 2011a,b; Tsugawa et al., 2011), also with additional GPS stations in the Asia-Pacific region (Tsai et al., 2011). Their onset time was earlier than the expected arrival time of the internal gravity waves that propagated from the surface to the ionosphere. This suggests that the wave propagated first as acoustic waves and excited internal gravity waves in the upper atmosphere. Spatial distribution of the ionospheric disturbances could accurately pinpoint the center of the seafloor uplift. Astafyeva et al. (2011) showed that the first pulse of the disturbance appeared only about 8 min after the earthquake, consistent with the travel time of the acoustic wave from the surface to the ionosphere. This was well before the tsunami hit the NE Japan coast and indicates that the GPS array is a promising sensor for the early warning system of tsunamis.

By studying the GPS array data from South Korea, Taiwan, and the Japanese GEONET, Chen et al. (2011) found the geomagnetic origin of directivity in the propagation of the acoustic waves in the ionosphere. Liu et al. (2011) identified Rayleigh wave-induced disturbances propagating with a speed of 2.3–3.3 km s⁻¹ using GPS receivers in Taiwan. Rolland et al. (2011a,b) and Galvan et al. (2012) analyzed the GPS data in Japan and identified three propagation speeds in the observed ionospheric disturbances and attributed them to gravity waves induced by tsunami (200–300 m s⁻¹) and direct acoustic waves (1000 m s⁻¹) and those excited by the Rayleigh waves (3400 m s⁻¹). Far-field data of the tsunami-induced ionospheric disturbances were, for the first time, observed by an airglow camera located in Hawaii (Makela et al., 2011), and Occhipinti et al. (2011) modeled these signals by internal gravity waves.

The atmospheric resonant oscillations were found to have lasted for 4 h by Saito et al. (2011) and Rolland et al. (2011b). They identified the 3.7 and 5.3 mHz oscillations in addition to the dominant 4.5 mHz oscillations, which were consistent with the frequencies of the atmospheric modes (Kobayashi,

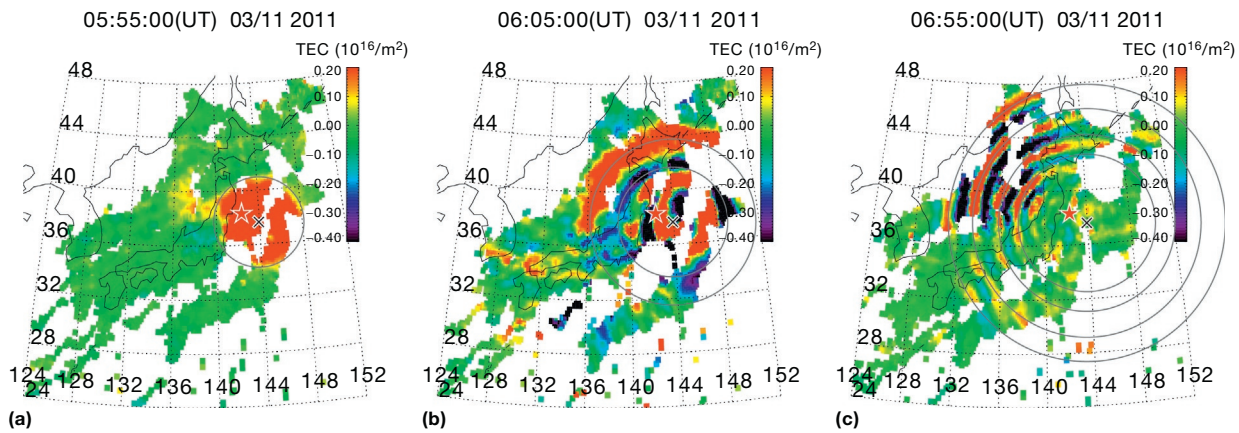


Figure 12 Two-dimensional maps of the detrended TEC at 05:55 UT (a), 06:05 UT (b), and 06:55 UT (c) on 11 March 2011. They show snapshots taken at about 10, 20, and 70 min after the earthquake, respectively. The star and cross marks represent the epicenter and the center of the ionospheric disturbance, respectively. Gray circles represent concentric circles from the center. A movie of the detrended TEC maps with 30 s resolution is available at the NICT website (<http://www.seg.nict.go.jp/2011TohokuEarthquake/>). Reproduced from Tsugawa T, Saito A, Otsuka Y, et al., (2011) Ionospheric disturbances detected by GPS total electron content observation after the 2011 off-the-Pacific coast of Tohoku Earthquake. *Earth, Planets and Space* 63: 875–879.

2007). These interpretations were substantiated by numerical simulations performed by Matsumura et al. (2011). This study was based on the 2-D simulation method of Shinagawa et al. (2007), which calculated the response of nonlinear, non-hydrostatic, compressible, and neutral atmosphere to impulsive vertical surface motion.

Various non-GPS sensors also detected disturbances in the troposphere and the ionosphere. A microbarograph in Oshu city, Iwate, successfully recorded infrasounds excited in the sea directly above the rupture area (Arai et al., 2011). This is considered to have propagated along the surface-atmosphere boundary as the Lamb wave. The lack of dispersion in the waveforms enabled the preservation of the original offshore waveforms of tsunami. An OTH SuperDARN in Hokkaido, Japan, also detected the ionospheric disturbances caused by this earthquake (Nishitani et al., 2011). Conventional sensors such as ionosonde were also used to study the ionospheric disturbances (Liu and Sun, 2011; Maruyama et al., 2011, 2012).

Several new phenomena were found after this earthquake. Postseismic formation of the ionospheric electron depletion (tsunamigenic ionospheric hole) was found and modeled by Saito et al. (2011) and Kakinami et al. (2012). TEC changes starting 1 h before megathrust earthquakes were suggested by Heki (2011). The same phenomenon was found to have occurred prior to the 2007 Bengkulu earthquake, Indonesia, by Cahyadi and Heki (2013).

4.16.3.7 Sources in the Atmosphere

Atmospheric events that generate infrasounds or gravity waves radiate in some cases enough energy to induce seismic signals through a dynamic coupling, and the inverse energy flow from the atmosphere to the solid Earth can occur. Two main categories are discussed in the succeeding text: volcanic eruptions and sonic booms. The latter include data from the shuttle, supersonic jets, or meteors that enter into the atmosphere.

4.16.3.7.1 Eruptions

Atmospheric waves produced by the Krakatoa eruption in 1883 were observed worldwide by barometric measurements. The propagation of such atmospheric disturbances is similar to those produced by nuclear explosions, and investigations were made in the 1960s to characterize these waves and their impact on the ionosphere (Harkrider and Press, 1967; Row, 1967). Following the eruption of Mount St. Helens in 1980, Roberts et al. (1982) detected a long-lived, large-scale traveling ionospheric disturbance in TEC measurements. Bolt and Tanimoto (1980) reported airwaves in barographic records that circled more than once around the globe.

The eruption of Mount Pinatubo (Philippines) on 15 June 1991 provided a remarkable example of the interaction between the solid and gaseous envelopes of the Earth system. The energy released in several explosions is estimated to be more than 100MT (TNT), generating significant atmospheric pressure waves (see Figure 6). Signals related to these waves were observed worldwide in barographs, ionograms, Doppler soundings, TEC measurements, and seismic data, resulting in multitude of analyses for different data. Igarashi et al. (1994) used the Japanese ionospheric observation network to determine the characteristics of the gravity wave and the associated traveling ionospheric disturbances. Kanamori et al. (1994) investigated the source mechanism of atmospheric oscillations from both barographic and seismographic records. Watada and Kanamori (2009) performed theoretical investigation on the resonance between the atmosphere and the lithosphere for periods 230 and 270 s that may occur following volcanic explosions. Johnson (2003) gave a review of infrasound observations emitted from volcanic eruptions and pointed out that it is useful to distinguish regular seismic signals related to subsurface seismicity from the seismicity associated with gas release.

Just like ionospheric disturbances caused by earthquakes, analysis of GPS-TEC data has been shown useful to study ionospheric disturbances by volcanic eruptions. Heki (2006) inferred the explosion energy associated with the September

2004 eruption of Mount Asama using GEONET data, by comparing the amplitudes of the disturbances with those by a mine blast of known explosion energy (Calais et al., 1998). Later, Dautermann et al. (2009a,b) improved the method to estimate the energy and applied it to the 2003 eruption of the Soufrière Hills volcano in the Lesser Antilles.

4.16.3.7.2 Sonic boom

Seismic and underwater perturbations induced by aircraft sonic booms have been studied since the mid-1960s (Cook et al., 1972). The frequency range is much higher than those for previously discussed phenomena. It should be noted that these sonic booms are one of the rare examples of controlled sources. The main effects of sonic booms arise in the waveforms of the strain with the shape of the N-wave overpressure and also in air-coupled Rayleigh wave trains following each N-wave transient. Seismic waves generated by the coupling can then propagate, faster than the original shock wave (Ishihara et al., 2003). More recently, the Concorde (LePichon et al., 2003) and the Space Shuttle provided further opportunities of studying those effects (Sorrells et al., 2002). Using seismic records of the sonic boom by the space shuttle Columbia, returning to the California Edwards Air Force base, Kanamori et al. (1991) observed P-wave pulse across the Los Angeles Basin, probably excited through the motion of high-rise buildings in response to the sonic boom. Yamamoto et al. (2011) observed audible sound, infrasound, and seismic data after the reentry of the Hayabusa sample capsule and the fragmented parts of the spacecraft in 13 June 2010.

Sonic boom was also shown to induce ionospheric perturbations through the atmosphere–ionosphere coupling using GPS data (Calais and Minster, 1998). Water vapor in the rocket exhaust causes large-scale electron depletions due to chemical reaction. Because their signatures are dominant in GPS-TEC data (Furuya and Heki, 2008; Ozeki and Heki, 2010), GPS is not necessarily a desirable tool to study acoustic disturbances, especially by ascending objects.

4.16.4 Conclusion

It has been a traditional practice for seismologists to ignore the atmosphere, the outermost layer of the Earth. To a large extent, this has been justified because of its relatively small effect on seismograms.

On the other hand, because of the existence of the atmospheric layer, we receive some benefits. In addition to understanding the causes of noise, which shed some light on the mechanism in the atmosphere–ocean–solid Earth interactions, one of the recent benefits has been the development of the correlation technique that allows us to retrieve Green's functions among pairs of stations. We can now obtain Green's functions for the solid Earth from the portions of seismograms that do not contain earthquake signals. This owes to the existence of noise and the development of theory on diffuse wavefield generated by noise.

Extending the analysis to include the atmospheric layer will increase opportunities to detect signals that are potentially useful for quantitative analysis of solid Earth processes. Volcanic eruption is an obvious process as it directly generates

atmospheric waves. Direct tsunami observation is also possible as surface displacement of ocean is not small and there are atmospheric waves that are coupled to this phenomenon. Shallow earthquakes also emit waves into the atmosphere, which may become a useful source of information. We have probably scratched only the surface of a large body of useful phenomena in the atmosphere, and as we develop the understanding of waves in the whole Earth system, we may discover many things that seismologists have missed in the past 100 years.

References

- Afraimovich EL, Perevalova NP, Plotnikov AV, and Uralov AM (2001) The shock-acoustic waves generated by earthquakes. *Annals of Geophysics* 19: 395–409.
- Aki K (1957) Space and time spectra of stationary stochastic waves, with special reference to microtremors. *Bulletin of the Earthquake Research Institute* 35: 415–456.
- Aki K (1965) A note on the use of microseisms in determining the shallow structures of the Earth's crust. *Geophysics* 30: 665–666.
- Arai N, Iwakuni M, Watada S, Imanishi Y, Murayama T, and Nogami M (2011) Atmospheric boundary waves excited by the tsunami generation related to the 2011 great Tohoku-Oki earthquake. *Geophysical Research Letters* 38: L00G18. <http://dx.doi.org/10.1029/2011GL049146>.
- Arduhin F, Stutzmann E, Schimmel M, and Mangeny A (2011) Ocean wave sources of seismic noise. *Journal of Geophysical Research* 116: C09004. <http://dx.doi.org/10.1029/2011JC006952>.
- Arendt S and Fritts DC (2000) Acoustic radiation by ocean surface waves. *Journal of Fluid Mechanics* 415: 1–21.
- Artru J, Ducic V, Kanamori H, Lognonné P, and Murakami M (2005) Ionospheric detection of gravity waves induced by Tsunamis. *Geophysical Journal International* 160(3): 840–848.
- Artru J, Farges T, and Lognonné P (2004) Acoustic waves generated from seismic surface waves: Propagation properties determined from Doppler sounding observations and normal-mode modeling. *Geophysical Journal International* 158(3): 1067–1077.
- Artru J, Lognonné P, and Blanc E (2001) Normal modes modeling of post-seismic ionospheric oscillations. *Geophysical Research Letters* 28(4): 697–700.
- Astafeyeva E and Heki K (2009) Dependence of waveform of near-field coseismic ionospheric disturbances on focal mechanisms. *Earth, Planets and Space* 61: 939–943.
- Astafeyeva E, Heki K, Kiryushkin V, Afraimovich E, and Shalimov S (2009) Two-mode long-distance propagation of coseismic ionosphere disturbances. *Journal of Geophysical Research* 114: A10307. <http://dx.doi.org/10.1029/2008JA013853>.
- Astafeyeva E, Lognonné P, and Rolland L (2011) First ionosphere images for the seismic slip of the Tohoku-oki Earthquake. *Geophysical Research Letters* L22104. <http://dx.doi.org/10.1029/2011GL049623>.
- Balasis G and Manda M (2007) Can electromagnetic disturbances related to the recent great earthquakes be detected by satellite magnetometers? *Tectonophysics* 431: 173–195.
- Bedard R, Lognonné P, Montagner JP, Cacho S, Karczewski JF, and Morand M (1996) The effects of the atmospheric pressure changes on seismic signals or how to improve the quality of a station. *Bulletin of the Seismological Society of America* 86(6): 1760–1769.
- Bedard AJ (2000) Atmospheric infrasound. *Physics Today* 53: 32–37.
- Ben-Menahem A (1975) Source parameters of the Siberia explosion of June, 1908, from analysis and synthesis of seismic signals at four stations. *Physics of the Earth and Planetary Interiors* 11: 1–35.
- Beroza G and Jordan T (1990) Searching for slow and silent earthquakes using free oscillations. *Journal of Geophysical Research* 95: 2485–2510.
- Bilitza D (2000) International reference ionosphere 2000. *Radio Science* 36(2): 261–275.
- Blanc E (1985) Observations in the upper atmosphere of infrasonic waves from natural or artificial sources: A summary. *Annals of Geophysics* 3(6): 673–688.
- Bolt B (1964) Seismic air waves from the great Alaska earthquake. *Nature* 202: 1095–1096.
- Bolt BA and Tanimoto T (1980) Atmospheric oscillations after the May 18, 1980 eruption of Mount St. Helens. *Eos* 62(23): 529.

- Boy JP, Hinderer J, and Gegout P (1998) Global atmospheric loading and gravity. *Physics of the Earth and Planetary Interiors* 109: 161–177.
- Briggs RW, Sieh K, Meltzer AJ, et al. (2006) Deformation and slip along the Sunda Megathrust in the great 2005 Nias-Simeulue earthquake. *Science* 311: 1897–1901.
- Bromirski PD (2001) Vibrations from the “Perfect Storm”. *Geochemistry, Geophysics, Geosystems* 2: 1030, Paper number: 2000GC000119.
- Bromirski PD and Duennebieer FK (2002) The near-coastal microseism spectrum: Spatial and temporal wave climate relationships. *Journal of Geophysical Research* 107(B8): 2166. <http://dx.doi.org/10.1029/2001JB000265>.
- Bromirski PD, Flick RE, and Graham N (1999) Ocean wave height determined from inland seismometer data: Implications for investigating wave climate change in the NE Pacific. *Journal of Geophysical Research* 104(C9): 20753–20766.
- Bromirski PD and Gerstoft P (2009) Dominant source regions of the Earth’s “hum” are coastal. *Geophysical Research Letters* 36: L13303. <http://dx.doi.org/10.1029/2009GL038903>.
- Bromirski PD, Sergienko OV, and MacAyeal DR (2010) Transoceanic infragravity waves impacting Antarctic ice shelves. *Geophysical Research Letters* 37: L02502. <http://dx.doi.org/10.1029/2009GL041488>.
- Bromirski PD and Stephen RA (2012) Response of the Ross Ice Shelf to ocean gravity wave forcing. *Annals of Glaciology* 53: 163–172.
- Cahyadi MN and Heki K (2013) Ionospheric disturbances of the 2007 Bengkulu and the 2005 Nias earthquakes, Sumatra, observed with a regional GPS network. *Journal of Geophysical Research* 118: 1–11. <http://dx.doi.org/10.1002/jgra.50208>.
- Calais E and Minster B (1995) GPS detection of ionospheric perturbations following the January 17, 1994, Northridge earthquake. *Geophysical Research Letters* 22(9): 1045–1048.
- Calais E and Minster B (1998) GPS, earthquakes, the ionosphere, and the Space Shuttle. *Physics of the Earth and Planetary Interiors* 105(3–4): 167–181.
- Calais E, Minster JB, Hofton MA, and Hedlin H (1998) Ionospheric signature of surface mine blasts from Global Positioning System measurements. *Geophysical Journal International* 132: 191202.
- Campillo M and Paul A (2003) Long range correlations in the diffuse seismic coda. *Science* 299: 547–549.
- Capon J (1972) Long-period signal processing results for LASA, NORSAR and ALPA. *Geophysical Journal of the Royal Astronomical Society* 31: 279–296.
- Cessaro RK (1994) Sources of primary and secondary microseisms. *Bulletin of the Seismological Society of America* 84(1): 142–148.
- Chen CH, Saito A, Lin CH, et al. (2011) Long-distance propagation of ionospheric disturbance generated by the 2011 off the Pacific coast of Tohoku Earthquake. *Earth, Planets and Space* 63: 881–884.
- Choosakul N, Saito A, Iyemori T, and Hashizume M (2009) Excitation of 4-min periodic ionospheric variations following the great Sumatra-Andaman earthquake in 2004. *Journal of Geophysical Research* 114: A10313. <http://dx.doi.org/10.1029/2008JA013915>.
- Cook JC, Gorchoth T, and Cook RK (1972) Seismic and underwater responses to sonic boom. *Journal of the Acoustical Society of America* 51(2): 729–741.
- Cooper RIB and Longuet-Higgins MS (1951) An experimental study of the pressure variations in standing water waves. *Proceedings of the Royal Society of London A* 206: 424–435.
- Coïsson P, Occhipinti G, Lognonné P, and Rolland LM (2011) Tsunami signature in the ionosphere: The innovative role of OTH radar. *Radio Science* 46: RS0D20. <http://dx.doi.org/10.1029/2010RS004603>.
- Crossley DJ, Jensen OG, and Hinderer J (1995) Effective barometric admittance and gravity residuals. *Physics of the Earth and Planetary Interiors* 90: 221–241.
- DasGupta A, Das A, Hui D, Bandyopadhyay KK, and Sivaraman MR (2006) Ionospheric perturbations observed by the GPS following the December 26th, 2004 Sumatra-Andaman earthquake. *Earth, Planets and Space* 58(2): 167–172.
- Dautermann T, Calais E, Lognonné P, and Mattioli GS (2009a) Lithosphere-atmosphere-ionosphere coupling after the 2003 explosive eruption of the Soufriere Hills Volcano, Montserrat. *Geophysical Journal International* 179: 1537–1546.
- Dautermann T, Calais E, and Mattioli GS (2009b) Global Positioning System detection and energy estimation of the ionospheric wave caused by the 13 July 2003 explosion of the Soufriere Hills Volcano, Montserrat. *Journal of Geophysical Research* 114: B02202. <http://dx.doi.org/10.1029/2008JB005722>.
- Davies K (1962) The measurement of ionospheric drifts by means of a Doppler shift technique. *Journal of Geophysical Research* 67: 4909–4913.
- Davies JB and Archambeau CB (1998) Modeling of atmospheric and ionospheric disturbances from shallow seismic sources. *Physics of the Earth and Planetary Interiors* 105: 183–199.
- Davies K and Baker DM (1965) Ionospheric effects observed around the time of the Alaskan earthquake of March 28, 1964. *Journal of Geophysical Research* 70: 1251–1253.
- Dolenc D, Romanowitz B, McGill P, and Wilcock W (2008) Observations of infragravity waves at the ocean-bottom broadband seismic stations Endeavour (KEBB) and Explorer (KXBB). *Geochemistry, Geophysics, Geosystems* 9: Q05007. <http://dx.doi.org/10.1029/2008GC001942>.
- Donn W and Naini B (1973) Sea wave origin of microbaroms and microseisms. *Journal of Geophysical Research* 78(21): 4482–4488.
- Donn W and Posmentier ES (1964) Ground-coupled air waves from the great Alaskan earthquake. *Journal of Geophysical Research* 69: 5357.
- Drob DP, Picone JM, and Garces M (2003) Global morphology of infrasound propagation. *Journal of Geophysical Research* 108(D21): 4680.
- Ducic V, Artru J, and Lognonné P (2003) Ionospheric remote sensing of the Denali Earthquake Rayleigh surface waves. *Geophysical Research Letters* 30: 1951. <http://dx.doi.org/10.1029/2003GL017812>.
- Duvall TL, Jefferies SM, Harvey JW, and Pomerantz M (1993) Time–distance helioseismology. *Nature* 362: 430–432.
- Dziewonski AM and Anderson DL (1981) Preliminary reference Earth model. *Physics of the Earth and Planetary Interiors* 25: 297–356.
- Ekström G (2001) Time domain analysis of Earth’s long-period background seismic radiation. *Journal of Geophysical Research* 106(B11): 26483–26493.
- Friedrich A, Kruger F, and Klinge K (1998) Ocean-generated microseismic noise located with the Grafenberg array. *Journal of Seismology* 2: 47–64.
- Fukao Y, Nishida K, Suda N, Nawa K, and Kobayashi N (2002) A theory of the earth’s background free oscillations. *Journal of Geophysical Research* 107(B9): 2206. <http://dx.doi.org/10.1029/2001JB000153>.
- Furuya T and Heki K (2008) Ionospheric hole behind an ascending rocket observed with a dense GPS array. *Earth, Planets and Space* 60: 235–239.
- Galvan DA, Komjathy A, Hickey MP, et al. (2012) Ionospheric signatures of Tohoku–Oki tsunami of March 11, 2011: Model comparisons near the epicenter. *Radio Science* 47: 4003. <http://dx.doi.org/10.1029/2012RS005023>.
- Galvan DA, Komjathy A, Mickey MP, and Mannucci AJ (2011) The 2009 Samoa and 2010 Chile tsunamis as observed in the ionosphere using GPS total electron content. *Journal of Geophysical Research* 116: A06318. <http://dx.doi.org/10.1029/2010JA016204>.
- Garces M, Caron P, Hetzer C, et al. (2005) Deep infrasound from the Sumatra earthquake and tsunami. *Eos, Transactions of the American Geophysical Union* 86(35): 317–320.
- Garces M, Hetzer C, Merrifield M, Willis M, and Aucan J (2003) Observations of surf infrasound in Hawaii. *Geophysical Research Letters* 30(24): 2264–2267. <http://dx.doi.org/10.1029/2003GL018614>.
- Garcia R, Crespon F, Ducic V, and Lognonné P (2005) Three-dimensional ionospheric tomography of post-seismic perturbations produced by the Denali earthquake from GPS data. *Geophysical Journal International* 163: 1049–1064.
- Gerstoft P and Tanimoto T (2007) A year of microseisms in Southern California. *Geophysical Research Letters* 34: L20304. <http://dx.doi.org/10.1029/2007GL031091>.
- Goldreich P and Keeley AD (1977) Solar Seismology II. The stochastic excitation of the solar P-modes by turbulent convection. *Astrophysical Journal* 212: 243–251.
- Graces MA (1997) On the volcanic waveguide. *Journal of Geophysical Research* 102(B10): 22547–22564.
- Grevemeyer I, Herber R, and Essen H-H (2000) Microseismological evidence for a changing wave climate in the northeast Atlantic Ocean. *Nature* 408: 349–352.
- Gusman AR, Tanioka Y, Kobayashi T, Latief H, and Pandoe W (2010) Slip distribution of the 2007 Bengkulu earthquake inferred from tsunami waveforms and InSAR data. *Journal of Geophysical Research* 115: B12316. <http://dx.doi.org/10.1029/2010JB007565>.
- Gutenberg B (1958) Two types of microseisms. *Journal of Geophysical Research* 63: 595–597.
- Hagerty MT, Kim WY, and Martysevich P (2002) Infrasound detection of large mining blasts in Kazakhstan. *Pure and Applied Geophysics* 159: 1063–1079.
- Harkrider D and Press F (1967) The Krakatoa air–sea waves: An example of pulse propagation in coupled systems. *Geophysical Journal of the Royal Astronomical Society* 13: 149–159.
- Hasselmann K (1963) A statistical analysis of the generation of microseisms. *Reviews of Geophysics* 1(2): 177–210.
- Haubrich RA, Munk W, and Snodgrass FE (1963) Comparative spectra of microseisms and swell. *Bulletin of the Seismological Society of America* 53: 27–37.
- Heki K (2006) Explosion energy of the 2004 eruption of the Asama Volcano, central Japan, inferred from ionospheric disturbances. *Geophysical Research Letters* 33: L14303. <http://dx.doi.org/10.1029/2006GL026249>.
- Heki K (2011) Ionospheric electron enhancement preceding the 2011 Tohoku–Oki earthquake. *Geophysical Research Letters* 38: L17312. <http://dx.doi.org/10.1029/2011GL047908>.

- Heki K, Otsuka Y, Choosakul N, Hemmakorn N, Komolmis T, and Maruyama T (2006) Detection of ruptures of Andaman fault segments in the 2004 great Sumatra earthquake with coseismic ionospheric disturbances. *Journal of Geophysical Research* 111: B09313. <http://dx.doi.org/10.1029/2005JB004202>.
- Heki K and Ping J (2005) Directivity and apparent velocity of the coseismic traveling ionospheric disturbances observed with a dense GPS network. *Earth and Planetary Science Letters* 236: 845–855.
- Hickey MP, Schubert G, and Walterscheid RL (2009) Propagation of tsunami-driven gravity waves into the thermosphere and ionosphere. *Journal of Geophysical Research* 114: A08304. <http://dx.doi.org/10.1029/2009JA014105>.
- Hickey MP, Schubert G, and Walterscheid RL (2010) Atmospheric airglow fluctuations due to a tsunami-driven gravity wave disturbance. *Journal of Geophysical Research* 115: A06308. <http://dx.doi.org/10.1029/2009JA014977>.
- Hillers G, Graham N, Campillo M, Kedar S, Landés M, and Shapiro N (2012) Global oceanic microseism sources as seen by seismic arrays and predicted by wave action models. *Geochemistry, Geophysics, Geosystems* 2(13): Q01021. <http://dx.doi.org/10.1029/2011GC003875>.
- Hinderer J and Crossley D (2000) Time variations in gravity and inferences on the Earth's structure and dynamics. *Surveys in Geophysics* 21: 1–45.
- Hines CO (1960) Internal atmospheric gravity waves at ionospheric heights. *Canadian Journal of Physics* 38: 1441–1481.
- Hines CO (1972) Gravity-waves in atmosphere. *Nature* 239: 73–78.
- Igarashi K, Kaminuma S, Nishimuta I, et al. (1994) Ionosphere and atmospheric disturbances around Japan caused by the eruption of Mount-Pinatubo on 15 June, 1991. *Journal of Atmospheric and Terrestrial Physics* 56: 1227–1234.
- Il-Young C, Jun M-S, Jeon J-S, and Min KD (2002) Analysis of local seismo-acoustic events in the Korean peninsula. *Geophysical Research Letters* (29). <http://dx.doi.org/10.1029/2001GL014060>.
- Ishihara Y, Tsukada S, Sakai S, Hiramatsu Y, and Furumoto M (2003) The 1998 Miyako fireballs trajectory determined from shock wave records of a dense seismic array. *Earth, Planets and Space* 55: 9–12.
- Iyemori T, Nose M, Han D, et al. (2005) Geomagnetic pulsations caused by the Sumatra earthquake on December 26, 2004. *Geophysical Research Letters* 32: L20807. <http://dx.doi.org/10.1029/2005GL024083>.
- Johnson JB (2003) Generation and propagation of infrasonic airwaves from volcanic explosions. *Journal of Volcanology and Geothermal Research* 121: 1–14.
- Kakinami Y, Kamogawa M, Tanioka Y, et al. (2012) Tsunamigenic ionospheric hole. *Geophysical Research Letters* 39: L00G27. <http://dx.doi.org/10.1029/2011GL050159>.
- Kanamori H, Mori J, Anderson DL, and Heaton TH (1991) Seismic excitation by the space-shuttle Columbia. *Nature* 349: 781–782.
- Kanamori H, Mori J, and Harkrider D (1994) Excitation of atmospheric oscillations by volcanic eruptions. *Journal of Geophysical Research* 22: 21947–21961.
- Kedar S, Longuet-Higgins MS, Webb FH, Graham N, Clayton RW, and Jones CE (2008) The origin of deep ocean microseisms in the North Atlantic Ocean. *Proceedings of the Royal Society A* 464(2091): 777–793. <http://dx.doi.org/10.1098/rspa.2007.0277>.
- Kobayashi N (2007) A new method to calculate normal modes. *Geophysical Journal International* 168: 315–331.
- Kobayashi N and Nishida K (1998) Continuous excitation of planetary free oscillations by atmospheric disturbances. *Nature* 395: 357–360.
- Lacoss RT, Kelly EJ, and Toksoz MN (1969) Estimation of seismic noise structure using seismic arrays. *Geophysics* 34(1): 21–38.
- Landau LD and Lifshitz EM (1987) *Fluid Mechanics*. Elmford, New York, USA: Pergamon Press.
- Lanyi GE and Roth E (1988) A comparison of mapped and measured total ionospheric electron content using global positioning system and beacon satellite observation. *Radio Science* 23: 483–492.
- Lay T, Kanamori H, Ammon CJ, et al. (2005) The great Sumatra–Andaman earthquake of 26 December 2004. *Science* 308(5725): 1127–1133. <http://dx.doi.org/10.1126/science.1112250>.
- Le Pichon A, Herry P, Mialle P, et al. (2005) Infrasound associated with 2004–2005 large Sumatra earthquakes and tsunamis. *Geophysical Research Letters* 32: L19802. <http://dx.doi.org/10.1029/2005GL023893>.
- Lee AW (1935) On the direction of approach of microseismic waves. *Proceedings of the Royal Society of London. Series A: Mathematical and Physical Sciences* 149(866): 183–199.
- LePichon A, Guilbert J, Vallee M, Dessa JX, and Ulziibat M (2003) Infrasonic imaging of the Kunlun mountains for the great 2001 China earthquake. *Geophysical Research Letters* 30: 1814.
- LePichon A, Guilbert J, Vega A, Garces M, and Brachet N (2002) Ground-coupled air waves and diffracted infrasound from the Arequipa earthquake of June 23, 2001. *Geophysical Research Letters* 29: 1886–1889.
- Liu JY, Chen CH, Lin CH, Tsai HF, Chen CH, and Kamogawa M (2011) Ionospheric disturbances triggered by the 11 March 2011 M9.0 Tohoku earthquake. *Journal of Geophysical Research* 116: A06319. <http://dx.doi.org/10.1029/2011JA016761>.
- Liu JY and Sun YY (2011) Seismo-traveling ionospheric disturbances of ionograms observed during the 2011 Mw 9.0 Tohoku Earthquake. *Earth, Planets and Space* 63: 897–902.
- Liu JY, Tsai YB, Chen SW, et al. (2006a) Giant ionospheric disturbances excited by the M9.3 Sumatra earthquake of 26 December 2004. *Geophysical Research Letters* 33: L02103. <http://dx.doi.org/10.1029/2005GL023963>.
- Liu J-Y, Tsai Y-B, Ma K-F, et al. (2006b) Ionospheric GPS total electron content (TEC) disturbances triggered by the 26 December 2004 Indian Ocean tsunami. *Journal of Geophysical Research* 111: A05303. <http://dx.doi.org/10.1029/2005JA011200>.
- Lobkis O and Weaver R (2001) On the emergence of the Green's function in the correlations of a diffuse field. *Journal of the Acoustical Society of America* 110: 3011–3017.
- Lognonné P, Clevede E, and Kanamori H (1998) Computation of seismograms and atmospheric oscillations by normal-mode summation for a spherical Earth model with realistic atmosphere. *Geophysical Journal International* 135: 388–406.
- Longuet-Higgins MS (1950) A theory of the origin of microseisms. *Philosophical Transactions of the Royal Society of London, Series A* 243: 1–35.
- Mai CL and Kiang JF (2009) Modeling of ionospheric perturbation by 2004 Sumatra tsunami. *Radio Science* 44: RS3011. <http://dx.doi.org/10.1029/2008RS004060>.
- Makela JJ, Lognonné P, Hebert H, et al. (2011) Imaging and modeling the ionospheric airglow response over Hawaii to the tsunami generated by the Tohoku earthquake of 11 March 2011. *Geophysical Research Letters* 38: L00G02. <http://dx.doi.org/10.1029/2011GL047860>.
- Mannucci AJ, Wilson BD, Yuan DN, Ho CH, Lindqwister UJ, and Runge TF (1998) A global mapping technique for GPS-derived ionospheric electron content measurements. *Radio Science* 33: 565–582.
- Maruyama T, Tsugawa T, Kato H, Ishii M, and Nishioka M (2012) Rayleigh wave signature in ionograms induced by strong earthquakes. *Journal of Geophysical Research* 117: A08306. <http://dx.doi.org/10.1029/2012JA017952>.
- Maruyama T, Tsugawa T, Kato H, Saito A, Otsuka Y, and Nishioka M (2011) Ionospheric multiple stratifications and irregularities induced by the 2011 off the Pacific coast of Tohoku Earthquake. *Earth, Planets and Space* 63: 869–873.
- Matsumura M, Saito A, Iyemori T, et al. (2011) Numerical simulations of atmospheric waves excited by the 2011 off the Pacific coast of Tohoku Earthquake. *Earth, Planets and Space* 63: 885–889.
- Meng L, Ampuero JP, Stock J, Duputel Z, Luo Y, and Tsai VC (2012) Earthquake in a maze: Compressional rupture branching during the 2012 Mw 8.6 Sumatra Earthquake. *Science* 337: 724–726.
- Merriam JB (1992) An ephemeris for gravity tide predictions at the nanogal level. *Geophysical Journal International* 108: 415–422.
- Mikumo T, Shibutani T, Le Pichon A, et al. (2008) Low-frequency acoustic-gravity waves from coseismic vertical deformation associated with the 2004 Sumatra–Andaman earthquake (Mw=9.2). *Journal of Geophysical Research* 113: B12402.
- Müller T and Zürn W (1983) Observation of gravity changes during the passage of cold fronts. *Journal of Geophysics* 53: 155–162.
- Mutschlecner JP and Whitaker RW (2005) Infrasound from earthquakes. *Journal of Geophysical Research* 110(D1): D01108.
- Najita K, Weaver PF, and Yuen PC (1973) A tsunami warning system using an ionospheric technique. *Proceedings of the IEEE* 62: 563–567.
- Najita K and Yuen PC (1979) Long-period oceanic Rayleigh wave group velocity dispersion curve from the Doppler sounding of the ionosphere. *Journal of Geophysical Research* 84: 1253–1260.
- Nawa K, Suda N, Fukao Y, Sato T, Aoyama Y, and Shibuya K (2000a) Incessant excitation of the Earth's free oscillations. *Earth, Planets and Space* 50: 3–8.
- Nawa K, Suda N, Fukao Y, et al. (2000b) Incessant excitation of the Earth's free oscillations: Global comparison of superconducting gravimeter records. *Physics of the Earth and Planetary Interiors* 120: 289–297.
- Nawa K, Suda N, Sato T, Aoyama Y, and Shibuya K (1998) Incessant excitation of the Earth's free oscillations. *Earth, Planets and Space* 50: 3–8.
- Niebauer TM (1998) Correcting gravity measurements for the effects of local air pressure. *Journal of Geophysical Research* 93(No. B7): 7989–7991.
- Nishida K, Fukao Y, Watada S, et al. (2005a) Array observation of background atmospheric waves in the seismic band from 1 mHz to 0.5 Hz. *Geophysical Journal International* 162: 824–840.
- Nishida K, Kobayashi N, and Fukao Y (2000) Resonant oscillations between the solid earth and the atmosphere. *Science* 287: 2244–2246.

- Nishida K, Kobayashi N, and Fukao Y (2002) Origin of Earth's ground noise from 2 to 20 mHz. *Geophysical Research Letters* 29(10). <http://dx.doi.org/10.1029/2001/GL013862>.
- Nishida K, Kobayashi N, and Fukao Y (2005b) Resonant oscillation between the solid Earth and the atmosphere. *Science* 287: 2244–2246.
- Nishida K, Montagner J, and Kawakatsu H (2009) Global surface wave tomography using seismic hum. *Science* 326: 112. <http://dx.doi.org/10.1026/science.1176389>.
- Nishitani N, Ogawa T, Otsuka Y, Hosokawa K, and Hori T (2011) Propagation of large amplitude ionospheric disturbances with velocity dispersion observed by the SuperDARN Hokkaido radar after the 2011 on the Pacific coast of Tohoku Earthquake. *Earth, Planets and Space* 63: 891–896.
- Occhipinti G, Coïsson P, Makela JJ, et al. (2011) Three-dimensional numerical modeling of tsunami-related internal gravity waves in the Hawaiian atmosphere. *Earth, Planets and Space* 63: 847–851.
- Occhipinti G, Dorey P, Farges T, and Lognonné P (2010) Nostradamus: The radar that wanted to be a seismometer. *Geophysical Research Letters* 37: L18104. <http://dx.doi.org/10.1029/2010GL044009>.
- Occhipinti G, Kherani EA, and Lognonné P (2008) Geomagnetic dependence of ionospheric disturbances induced by tsunamigenic internal gravity waves. *Geophysical Journal International* 173: 753–765.
- Occhipinti G, Lognonné P, Kherani EA, and Hebert H (2006) Three-dimensional waveform modeling of ionospheric signature induced by the 2004 Sumatra tsunami. *Geophysical Research Letters* 33: L20104. <http://dx.doi.org/10.1029/2006GL026865>.
- Okada H (2003) *The Microtremor survey method*. *Geophysical Monograph Series*, vol. 12. Society of Exploration Geophysicists. Washington D.C.: American Geophysical Union Monograph.
- Okihiro M, Guza R, and Seymour R (1992) Bound infragravity waves. *Journal of Geophysical Research* 97(C7): 11453–11469.
- Otsuka Y, Kotake N, Tsugawa T, et al. (2006) GPS detection of total electron content variations over Indonesia and Thailand following the 26 December 2004 earthquake. *Earth, Planets and Space* 58(2): 159–165.
- Ozeki M and Heki K (2010) Ionospheric holes made by ballistic missiles from North Korea detected with a Japanese dense GPS array. *Journal of Geophysical Research* 115: A09314. <http://dx.doi.org/10.1029/2010JA015531>.
- Peltier WR and Hines CO (1976) Possible detection of tsunamis by a monitoring of ionosphere. *Journal of Geophysical Research* 81: 1995–2000.
- Peterson J (1993) Observation and modeling of background seismic noise. *U.S. Geological Survey Open-File Report*. Albuquerque, NM.
- Phillips OM (1977) *The Dynamics of the Upper Ocean*. Cambridge: Cambridge University Press.
- Posmentier ES (1967) A theory of microbaroms. *Geophysical Journal of the Royal Astronomical Society* 13: 487–501.
- Prieto GA, Lawrence JF, and Beroza GC (2009) Anelastic Earth structure from the coherency of the ambient seismic field. *Journal of Geophysical Research* 114: B07303. <http://dx.doi.org/10.1029/2008JB006067>.
- Rabbel W and Zschau J (1985) Static deformations and gravity changes at the Earth's surface due to atmospheric loading. *Journal of Geophysics* 56: 81–99.
- Rhie J and Romanowicz B (2004) Excitation of Earth's continuous free oscillations by atmosphere-ocean-seafloor coupling. *Nature* 431: 552–556.
- Rickett J and Claerbout J (1999) Acoustic daylight imaging via spectral factorization: Helioseismology and reservoir monitoring. *The Leading Edge* 18: 957–960.
- Roberts DH, Klobuchar JA, Fougere PF, and Hendrickson DH (1982) A large amplitude travelling ionospheric disturbance produced by the May 18, 1980, explosion of Mount St. Helens. *Journal of Geophysical Research* 87: 6291–6301.
- Rolland LM, Lognonné P, Astafeyeva E, et al. (2011a) The resonant response of the ionosphere imaged after the 2011 off-the-Pacific coast of Tohoku Earthquake. *Earth, Planets and Space* 63: 853–857.
- Rolland LM, Lognonné P, and Munekane H (2011b) Detection and modeling of Rayleigh waves induced patterns in the ionosphere. *Journal of Geophysical Research* 116: A05320. <http://dx.doi.org/10.1029/2010JA016060>.
- Rolland L, Occhipinti G, Lognonné P, and Loevenbruck A (2010) The 29 September 2009 Samoan tsunami in the ionosphere detected off-shore Hawaii. *Geophysical Research Letters* 37: L17191. <http://dx.doi.org/10.1029/2010GL044479>.
- Roult G and Crawford W (2000) Analysis of 'background' free oscillations and how to improve resolution by subtracting the atmospheric pressure signal. *Physics of the Earth and Planetary Interiors* 121(3–4): 325–338.
- Roux P, Sabra KG, Gerstoft P, and Kupperman WA (2005a) P-waves from cross correlation of seismic noise. *Geophysical Research Letters* 32: L19303. <http://dx.doi.org/10.1029/2005GL023803>.
- Roux P, Sabra KG, Gerstoft P, Kupperman WA, and Roux A (2005b) Ambient noise cross correlation in free space: Theoretical approach. *Journal of the Acoustical Society of America* 117: 79–84. <http://dx.doi.org/10.1121/1.1830673>.
- Row RV (1967) Acoustic-gravity waves in the upper atmosphere due to a nuclear detonation and an earthquake. *Journal of Geophysical Research* 72: 1599–1610.
- Sabra KG, Gerstoft P, Roux P, and Kupperman WA (2005a) Extracting time-domain Green's function estimates from ambient seismic noise. *Geophysical Research Letters* 32: L03310. <http://dx.doi.org/10.1029/2004GL021862>.
- Sabra KG, Gerstoft P, Roux P, Kupperman WA, and Fehler M (2005b) Surface wave tomography from microseisms in Southern California. *Geophysical Research Letters* 32: L14311. <http://dx.doi.org/10.1029/2005GL023155>.
- Saito T (2010) Love-wave excitation due to the interaction between a propagating ocean wave and the sea-bottom topography. *Geophysical Journal International* 182: 1515–1523. <http://dx.doi.org/10.1111/j.1365-246X.2010.04695.x>.
- Saito A, Tsugawa T, Otsuka Y, et al. (2011) Acoustic resonance and plasma depletion detected by GPS total electron content observation after the 2011 off-the-Pacific coast of Tohoku Earthquake. *Earth, Planets and Space* 63: 863–867.
- Santo T (1960) Investigations into microseisms using the observational data of many stations in Japan (Part I) – On the origin of microseisms. *Bulletin of the Earthquake Research Institute* 37: 307–325.
- Sardon E, Rius A, and Zarrao N (1994) Estimation of the transmitter and receiver differential biases and the ionospheric total electron-content from Global Positioning System observations. *Radio Science* 29: 577–586.
- Schulte-Pelkum V, Earle PS, and Vernon FL (2004) Strong directivity of ocean-generated seismic noise. *Geochemistry, Geophysics, Geosystems* 5: Q03004. <http://dx.doi.org/10.1029/2003GC000520>.
- Shapiro N, Campillo M, Stehley L, and Ritzwoller M (2005) High-resolution surface-wave tomography from ambient seismic noise. *Science* 307: 1615–1618.
- Shinagawa H, Iyemori T, Saito S, and Maruyama T (2007) A numerical simulation of ionospheric and atmospheric variations associated with the Sumatra earthquake on December 26, 2004. *Earth, Planets and Space* 59: 1015–1026.
- Snieder R (2004) Extracting the Green's function from the correlation of coda waves: A derivation based on stationary phase. *Physical Review E* 69: 046610.
- Song YT, Ji C, Fu L-L, et al. (2005) The 26 December 2004 tsunami source estimated from satellite radar altimetry and seismic waves. *Geophysical Research Letters* 32: L20601. <http://dx.doi.org/10.1029/2005GL023683>.
- Sorrells GG (1971) A preliminary investigation into the relationship between long-period noise and local fluctuations in the atmospheric pressure field. *Geophysical Journal of the Royal Astronomical Society* 26: 71–82.
- Sorrells G, Bonner J, and Herrin ET (2002) Seismic precursors to space shuttle shock fronts. *Pure and Applied Geophysics* 159: 1153–1181.
- Sorrells G, McDonald J, Der Z, and Herrin E (1971) Earth motion caused by local atmospheric pressure changes. *Geophysical Journal of the Royal Astronomical Society* 26: 83–98.
- Spratt RS (1982) Modelling the effect of atmospheric pressure variations on gravity. *Geophysical Journal of the Royal Astronomical Society* 26: 83–98.
- Suda N, Nawa K, and Fukao Y (1998) Earth's background free oscillations. *Science* 279: 2089–2091.
- Sutton G and Barstow N (1996) Ocean bottom microseisms from a distant supertyphoon. *Geophysical Research Letters* 23(No. 5): 499–502.
- Tanimoto T (1999) Excitation of normal modes by atmospheric turbulence: Source of long-period seismic noise. *Geophysical Journal International* 136: 395–402.
- Tanimoto T (2005) The oceanic excitation hypothesis for the continuous oscillations of the Earth. *Geophysical Journal International* 160(1). <http://dx.doi.org/10.1111/j.1365-246X.2005.02491.x>.
- Tanimoto T (2007a) Excitation of normal modes by nonlinear interaction of ocean waves. *Geophysical Journal International* 168: 571–582. <http://dx.doi.org/10.1111/j.1365-246X.2006.03240.x>.
- Tanimoto T (2007b) Excitation of microseisms. *Geophysical Research Letters* 34: L05308. <http://dx.doi.org/10.1029/2006GL029046>.
- Tanimoto T and Um J (1999) Cause of continuous oscillations of the Earth. *Journal of Geophysical Research* 104(B12): 28273–28279.
- Tanimoto T, Um J, Nishida K, and Kobayashi N (1998) Earth's continuous oscillations observed on seismically quiet days. *Geophysical Research Letters* 25(10): 1553–1556.
- Tanioka Y, Yudhichara T, Kususe S, et al. (2006) Rupture process of the 2004 great Sumatra–Andaman earthquake estimated from tsunami waveforms. *Earth, Planets and Space* 58: 203–209.
- Tennekes H and Lumley JL (1972) *A First Course in Turbulence*. Cambridge, MA, USA: MIT Press.

- Traer J, Gerstoft P, Bromirski P, and Shearer P (2012) Microseisms and hum from ocean surface gravity waves. *Journal of Geophysical Research* 117: B11307. <http://dx.doi.org/10.1029/2012JB009550>.
- Tsai V (2011) Understanding the amplitudes of noise correlation measurements. *Journal of Geophysical Research* 116: B09311. <http://dx.doi.org/10.1029/2011JB008483>.
- Tsai HF, Liu JY, Lin CH, and Chen CH (2011) Tracking the epicenter and the tsunami origin with GPS ionosphere observation. *Earth, Planets and Space* 63: 859–862.
- Tsugawa T, Saito A, Otsuka Y, et al. (2011) Ionospheric disturbances detected by GPS total electron content observation after the 2011 off-the-Pacific coast of Tohoku Earthquake. *Earth, Planets and Space* 63: 875–879.
- Uchiyama Y and McWilliams JC (2008) Infragravity waves in the deep ocean: Generation, propagation, and seismic hum excitation. *Journal of Geophysical Research* 113: C07029. <http://dx.doi.org/10.1029/2007JC004562>.
- Van Dam TM and Wahr JM (1987) Displacement of the Earth's surface due to atmospheric loading: Effects on gravity and baseline measurements. *Journal of Geophysical Research* 92(B2): 1281–1286.
- van Tiggelen BA (2003) Green function retrieval and time reversal in a disordered world. *Physical Review Letters* 91: 243904.
- Virieux J, Garnier N, Blanc E, and Dessa JX (2004) Paraxial ray tracing for atmospheric wave propagation. *Geophysical Research Letters* 31: L20106.
- Warburton RJ and Goodkind JM (1977) The influence of barometric-pressure variations on gravity. *Geophysical Journal of the Royal Astronomical Society* 48: 281–292.
- Watada S and Kanamori H (2009) Acoustic resonant oscillations between the atmosphere and the solid Earth during the 1991 Mt. Pinatubo eruption. *Journal of Geophysical Research* 115: B12319. <http://dx.doi.org/10.1029/2010JB007747>.
- Watada S, Kunugi T, Hirata K, et al. (2006) Atmospheric pressure change associated with the 2003 Tokachi-Oki earthquake. *Geophysical Research Letters* 33: L24306. <http://dx.doi.org/10.1029/2006GL027967>.
- Watada S and Masters G (2001) Oceanic excitation of the continuous oscillations of the Earth. *Eos Transactions. American Geophysical Union* 82(47): SS2A-0620.
- Waxler R and Gilbert KE (2006) The radiation of atmospheric microbaroms by ocean waves. *Journal of the Acoustical Society of America* 119(1): 2651–2664. <http://dx.doi.org/10.1121/1.2191607>.
- Weaver R and Lobkis O (2001) Ultrasonics without a source: Thermal fluctuation correlations at MHz frequencies. *Physical Review Letters* 87: 134301.
- Webb S, Zhang X, and Crawford W (1991) Infragravity waves in the deep ocean. *Journal of Geophysical Research* 96(C2): 2723–2736.
- Whipple FJW (1930) The great Siberian meteor and the waves, seismic and aerial, which it produced. *Quarterly Journal of the Royal Meteorological Society* 56: 287–304.
- Widmer-Schmid R (2003) What can superconducting gravimeters contribute to normal-mode seismology? *Bulletin of the Seismological Society of America* 93(3): 1370–1380.
- Wielandt E and Steim JM (1986) A digital very-broadband seismograph. *Annals of Geophysics* 4B: 227–232.
- Woodhouse JH (1988) The calculation of the eigenfrequencies and eigenfunctions of the free oscillations of the Earth and the Sun. In: Doornbos DJ (ed.) *Seismological Algorithms: Computational Methods and Computer Programs*, pp. 321–370. London: Academic Press.
- Yamamoto M, Ishihara Y, Hiramatsu Y, et al. (2011) Detection of acoustic/infrasonic/seismic waves generated by hypersonic re-entry of the HAYABUSA capsule and fragmented parts of the spacecraft. *Proceedings of the Astronomical Society of Japan* 63: 971–978.
- Yeh KC and Liu CH (1972) *Theory of Ionospheric Waves*. New York: Academic Press.
- Young JM and Greene GE (1982) Anomalous infrasound generated by the Alaskan earthquake of 28 March 1964. *Journal of the Acoustical Society of America* 71: 334–339.
- Yuen PC, Weaver PF, Suzuki RK, and Furumoto AS (1969) Continuous travelling coupling between seismic waves and the ionosphere evident in May 1968 Japan earthquake data. *Journal of Geophysical Research* 74: 2256–2264.
- Zhang J, Gerstoft P, and Bromirski P (2010) Pelagic and coastal sources of P-wave microseisms: Generation under tropical cyclones. *Geophysical Research Letters* 37: L15301. <http://dx.doi.org/10.1029/2010GL044288>.
- Zürn W and Widmer R (1995) On noise reduction in vertical seismic records below 2 mHz using local barometric pressure. *Geophysical Research Letters* 22(24): 3537–3540.